Inorganic Mass Spectrometry

15

Learning Objectives

- Ionization of inorganic samples
- Elemental analysis by MS – special instrumentation
- Accurate isotopic compositions
- Lateral distribution of elements and mass spectral imaging
- Elemental MS for assessing biological systems
- Element speciation in organic materials and biological tissues

Mass spectrometry resulted from an endeavor to analyze gaseous ionic matter. The discovery of isotopes and the determination of their masses and relative abundances, i.e., *isotope ratios,* were a direct result of the pioneering work of Thomson, Aston, Dempster, and many others [1, 2]. Soon, the results of such measurements became the driving force for new discoveries in physics. The detection of mass defect, for example, was direct proof of the mass–energy equivalence as postulated by Einstein's special theory of relativity. It was not until the late 1940s that mass spectrometry was developed as a tool for the analysis of organic compounds, but within a decade or two, this branch flourished. In 1968, the journal *Organic Mass Spectrometry* was founded, and soon, the leap into *biomedical mass spectrometry* (also a journal title from 1974 to 1985) was taken. The majority of mass spectrometrists is now working in proteomics or metabolomics, in environmental, clinical and forensic trace analysis to name a few. Meanwhile, what became known as *inorganic mass spectrometry* [3–8] or *element mass spectrometry* has experienced equally revolutionary developments [9, 10] as its organic and biomedical counterpart – of which it could be considered a "sibling".

J.H. Gross, *Mass Spectrometry*, DOI 10.1007/978-3-319-54398-7_15

15.1 Concept and Techniques of Inorganic MS

The determination of molecular formulas via accurate mass measurements relies on isotopic masses accurate to at least 1 in 10^8 [11]. Elemental trace analysis is required for the detection of radioactive nuclides in the environment, of transition metals such as Pt in exhaust fumes from automobiles [12], and in the quality control of low-sulfur fuels for the same. All electronic devices demand for high-purity semiconductors and the properties of alloys are critically influenced by trace elements [13]. Age determinations from isotope ratios are applied in archeology, paleontology, and geology [4, 14, 15]. More recently, elemental MS and biomedical MS are jointly employed to unveil the presence and preferably location of metals in proteins or DNA as well as their lateral distribution in tissues [16–20], a field of research basically going back to seminal work by Houk in 1980 [21]. Moreover, the prominent role of metal ions in physiological processes gave rise to a new field of research: *metallomics* [22–24]. Finally, we are wittnessing a rapid expansion of imaging techniques based on former methods of element MS into the exploration of complex biological systems [25–28]. This altogether makes it mandatory to include at least a compact chapter on *inorganic mass spectrometry* in this book.

Inorganic mass spectrometry generally addresses either of the following analytical tasks:

- Determine the elemental composition of metals, alloys, rock samples, semiconductors, and other inorganic materials.
- Detect and quantify elements at low concentrations or trace levels in a sample.
- Detect and quantify trace isotopes in a sample.
- Image the lateral distribution of one or multiple elements in a sample.
- Determine the accurate mass of stable or radioactive isotopes.
- Determine the accurate isotopic composition of an element in a sample.

When accurate ratios of (stable) isotopes are to be determined, this is referred to as *isotope ratio mass spectrometry* (IR-MS; for the δ notation in IR-MS and an example of IR-MS cf. Sect. 3.1.6.) [3, 6–8]. While the techniques of inorganic MS are mainly referenced according to the ionization method in use, IR-MS describes the analytical approach. Thus, IR-MS may employ different ionization techniques, and vice versa, TIMS for example, may be employed in IR-MS (Table 15.1).

Both the reliable determination of isotope ratios and the quantitation of trace elements are generally accompanied by complete destruction of all molecular entities. Opposed to what is normally desired in organic and bio-organic mass spectrometry, ionization methods in inorganic mass spectrometry therefore use conditions which erase any molecular structure, i.e., inorganic mass spectrometry particularly employs high temperature plasmas to achieve atomization prior to ionization and mass analysis [29]. Furthermore, ion–neutral reactions need to be suppressed or their products destroyed in order to ensure isotopic patterns free from interferences with isobars [30, 31].

Table 15.1 Techniques in inorganic mass spectrometry

Acronym	Technique
IR-MS	Isotope ratio mass spectrometry
TIMS	Thermal ionization mass spectrometry
SSMS	Spark source mass spectrometry
GDMS	Glow discharge mass spectrometry
ICP-MS	Inductively coupled plasma mass spectrometry
LA-ICP-MS	Laser ablation-inductively coupled plasma mass spectrometry
SIMS	Secondary ion mass spectrometry
AMS	Accelerator mass spectrometry

It does not surprise that neither a single type of mass spectrometer nor a single method of ion generation can fulfill all of the requirements for measuring all varying sample types and compositions equally well. While accelerator mass spectrometers, for example, deliver very high abundance sensitivity and low background, they have low sample throughput and need larger amounts of sample. ICP mass spectrometers, on the other side, tend to have higher sample throughput while being more susceptible to isobaric interferences. These different types of instruments are best viewed as complementing each other in their analytical capabilities (Fig. 15.1) [32, 33].

Identification of metalloproteins The function of metalloproteins critically depends on their interaction with a metal, e.g., Cu, Zn, Fe, Mo, or metalloid such as Se or As. The living cell not only depends on its genome and proteome, but also on its metallome, i.e., the distribution of those elements among different biomolecules. It is estimated that about 30% of the proteome is made up by metalloproteins [24]. The complexity of speciation analysis demands for a combined approach of separation techniques and different methods of mass spectrometry. This is best illustrated by the metallomics toolbox that reflects the current understanding of how the metallome can be explored (Fig. 15.2) [23].

Speciation of selenium in yeast proteins The speciation of selenium incorporated in yeast proteins shows the high degree to which elemental and biomedical MS are interrelated by now. The analysis started with a tryptic digest of the water-soluble protein fraction that had been isolated by size-exclusion chromatography. Analysis of the digest by reversed-phase HPLC-*inductively coupled plasma mass spectrometry* (ICP-MS) provided identification of the selenopeptide fraction, which was then analyzed by MALDI-TOF-MS in order to select target ions for tandem MS. Finally, the sequences of the selected selenopeptides were derived from ESI-CID spectra. This combined approach using ICP-MS, MALDI-MS, and ESI-MS allowed for the first time the identification of the heat-shock protein HSP12 (M_r = 11,693 u) in which the only methionine residue was replaced by selenomethionine (Fig. 15.3) [34].

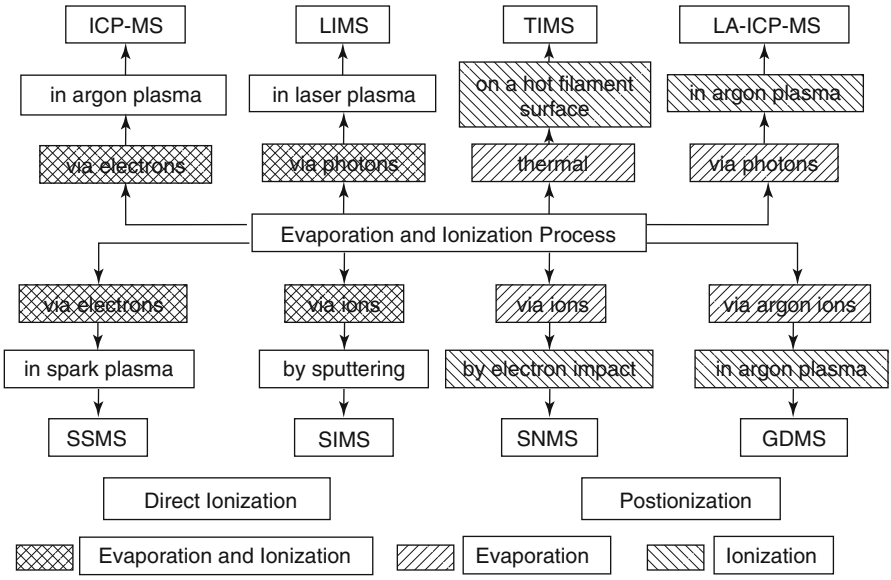

Fig. 15.1 Elemental MS techniques classified with respect to their evaporation and ionization processes (Reproduced from Ref. [32] with permission. © Elsevier Science Publishers, 2000)

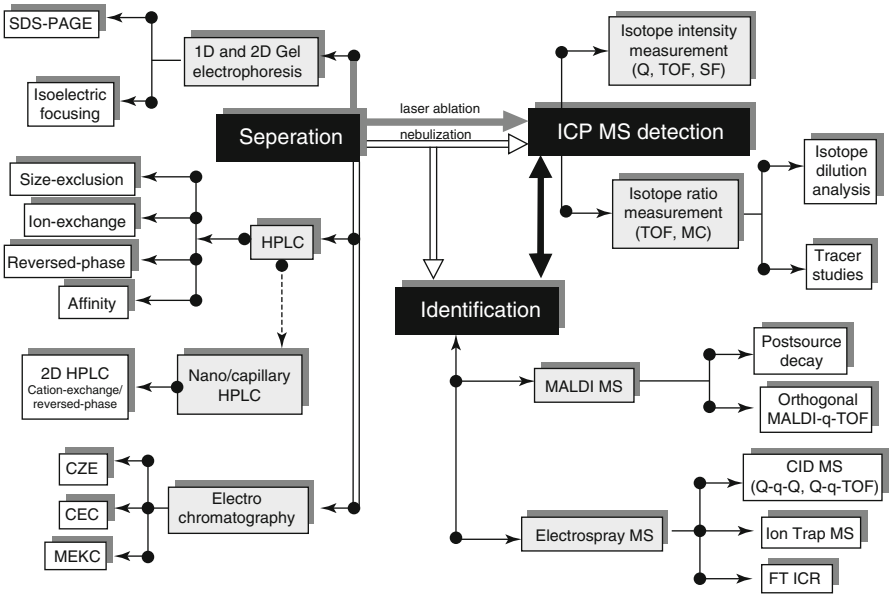

Fig. 15.2 The state-of-the art toolbox with hyphenated techniques for element speciation analysis and metallomics. The *upper right* section presents the tools of inorganic mass spectrometry (Reproduced from Ref. [23] with permission. © Wiley Periodicals Inc., 2006)

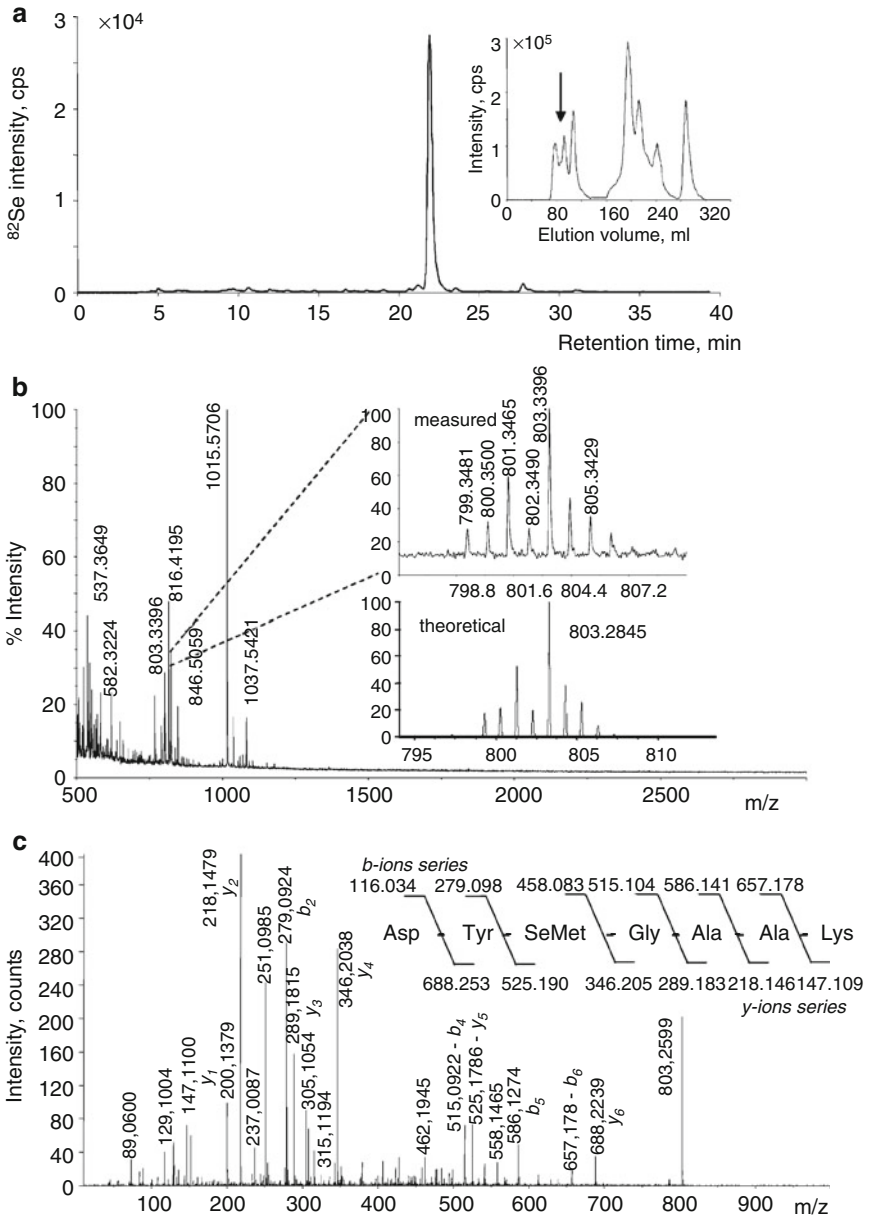

Fig. 15.3 Identification of the selenopeptide of the HSP12 protein: (**a**) Reconstructed ion chromatogram based on ^{77}Se and ^{82}Se from reversed-phase HPLC-ICP-MS of the Se-containing protein fraction (as obtained from the marked region in the size-exclusion chromatogram in the inset); (**b**) MALDI-TOF mass spectrum of the fraction producing the peak correlated to Se in part (**a**); (**c**) ESI-CID mass spectrum of the $[M + H]^+$ ion, *m/z* 803.25, of the selenopeptide (Reproduced from Ref. [34] with permission. © American Chemical Society, 2003)

15.2 Thermal Ionization Mass Spectrometry

Atomic and eventually molecular ions can be formed by *thermal ionization* (TI), also known as *surface ionization* (SI). For *thermal ionization mass spectrometry* (TI-MS), a metal salt, metal oxide, or metal is placed onto the surface of a rhenium or tungsten filament where it is heated in vacuum to 400–2300 °C. In practice, an assembly of one to three ribbon filaments in close proximity is employed for TI (Fig. 15.4). The first filament is loaded with the sample and heated to evaporate the analyte. The neutral atoms or molecules emerging thereof may then be ionized on the second filament. Electron transfer *to* the bulk metal results in positive ions while electron transfer *from* the filament yields anions. The third filament of a triple filament assembly is normally used to deliver a standard that can be analyzed alternating with the unknown under virtually identical ion source conditions. Double and triple filament assemblies have the advantage that evaporation and ionization temperature can be independently controlled. While evaporation is preferably performed at comparatively low temperature in order to obtain long-lasting signals and minor isotopic fractionation, ionization requires high temperatures for good ionization efficiency. Careful control of filament temperature [35] ensures that nanogram to microgram amounts of sample yield signals for hours because evaporation rates are in the order of picograms per second. Thoroughly chosen evaporation conditions are also vital for the reliability of the results [33]. Normally, 10–20 filament assemblies are mounted on one carousel-like sample turret in order to avoid frequent breaking of the vacuum. Once loaded and pumped to high vacuum, the instrument may be operated for days until all samples are measured.

Ion formation in TI relies on the blurring of the discrete electronic states of the neutral at high temperature. This way, the Fermi levels of adsorbed neutral and bulk metal can merge into a common band causing the charge state of the weakly surface-bound particle to be purely determined by Fermi statistics. In other words, as the electrons move freely between the adsorbed atom and the surface the atom is positive at times. Assuming ideal conditions, the degree of ionization,

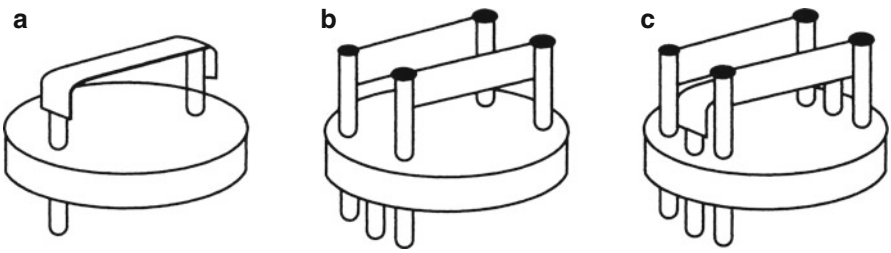

Fig. 15.4 From left (**a**) single filament, (**b**) double filament, and (**c**) triple filament assemblies for thermal ionization of metal salts and oxides (Reproduced from Ref. [3] with permission. © John Wiley & Sons Ltd., 1997)

i.e., the ratio of ions and neutrals leaving the surface, is described by the *Saha-Langmuir equation*. The degree of positive ionization α^+ is given as

$$\alpha^+ = \frac{N^+}{N^0} = \frac{g^+}{g^0}\exp\left[\frac{e\,(\Phi - IE)}{kT}\right] \tag{15.1}$$

$$= \frac{g^+}{g^0}\exp\left[1.16 \times 10^4 \frac{(\Phi - IE)}{T}\right] \tag{15.2}$$

where g^+/g^0 is the ratio of electronic states of the ion and the neutral, *IE* is the ionization energy of the atom or molecule to be ionized, Φ is the work function of the filament material, and *T* is the temperature of the ionizing filament. Best ionization efficiency is therefore obtained when metals of low *IE* are exposed to high temperature on filament materials that have large Φ. This is achieved by using filaments made of rhenium ($\Phi_{Re} = 4.98$ eV, *m.p.* = 3180 °C) or tungsten ($\Phi_W = 4.58$ eV, *m.p.* = 3410 °C; Fig. 15.5).

Vice versa, nonmetallic elements with high *IE* and metal oxides may form negative ions [36, 37]. The degree of ionization α^- is then obtained from the modified Saha-Langmuir equation

$$\alpha^- = \frac{g^-}{g^0}\exp\left[1.16 \times 10^4 \frac{(EA - \Phi)}{T}\right] \tag{15.3}$$

where *EA* is the electron affinity of the adsorbed atom.

Due to the low spatial and energetic spread of ions from TI, the method can be combined with single-focusing magnetic sector mass analyzers or quadrupoles [38]. Nonetheless, TI ion sources require dedicated instrumentation, frequently

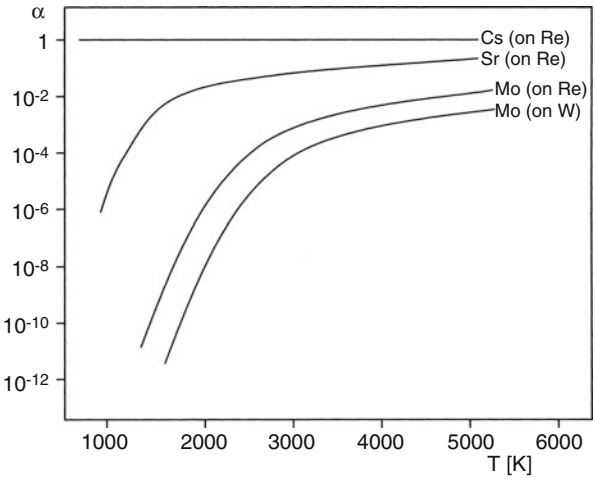

Fig. 15.5 Thermal ionization efficiency α^+ vs. filament temperature. The curves for Mo reflect the dependence of α^+ on the filament material. The advantage of the Re over the W filament follows from Eqs. 15.1–15.2 (Reproduced from Ref. [7] with permission. © John Wiley & Sons Ltd., 2008)

equipped with *multicollector* (MC) systems to insure the highest accuracy for the isotope ratios measured (Sects. 3.3.2 and 7.2 in [3]).

The favorite application of TI is *isotope ratio mass spectrometry* (IR-MS) and trace elemental analysis of metals and inorganic metal compounds. This is, however, in no way limiting the applicability of TI-MS to the elemental analysis of organic material including food. Such samples are transformed into suitable compounds by (extensive) work-up such as freeze-drying, oxidative treatment with concentrated HNO_3 or HNO_3/H_2O_2, ashing, or electrolytic deposition [39, 40]. TI of organic salts remained a rare exception [41]. TI-MS is not suitable for mixture analysis and multi-element determinations where ICP-MS is normally employed. Due to its high precision, TI-MS is important as a reference method to calibrate other techniques of isotope ratio MS, such as MC-ICP-MS that, while also requiring matrix separation, is still able to deliver higher sample throughput (Sect. 15.4). TI-MS also serves for the certification of reference materials because accuracy and precision of the method are excellent [42].

TI-MS or TIMS?
In the element MS community it is common to use the acronym TIMS without hyphen rather than the form TI-MS. The same is observed in case of other techniques employed for element MS, e.g., *secondary ion mass spectrometry* is abbreviated SIMS rather than SI-MS.

15.3 Spark Source Mass Spectrometry

The *spark source* (SS) developed by Dempster in 1935, provided the first truly multi-element and isotopic trace element method [43]. In *spark source mass spectrometry* (SS-MS), a solid sample is vaporized under vacuum by a high-voltage radiofrequency spark. The electric discharge is maintained between two pin-shaped electrodes (about 10 mm in length and 1–2 mm in diameter) in vacuum.

SS-MS is best suited for conducting samples, because the electrodes may then be directly prepared from the solid to be analyzed. Prior to insertion into the ion source, the electrodes have to be carefully cleaned, e.g., by etching, to avoid surface contamination (Sect. 5.2 in [6], Sect. 2.2 in [7]). If the sample is not itself conducting, high-purity graphite, or if neccessary silver or gold powder are used as scaffolding for the electrodes. Often, an *internal standard element* or an *isotopically enriched spike* are admixed to this powder before the finely ground analyte-containing material is added. Typically, 50 mg of powdered material, e.g., a rock sample, is mixed with the graphite powder and then compressed into electrode pins [44].

The detection limits for the elements from Rb through U generally vary between 0.001 and 0.1 ppm (equivalent to 0.001–0.1 μg g^{-1}). Certain elements such as Nb, Zr, Y, Sn, Sb, and Th can even be measured at the ppb (ng g^{-1}) level [45].

Trace ≠ small sample
Although an element may be detected at the ultratrace level by SS-MS, the amount of sample required is comparatively large since electrodes lasting for several hours of operation are needed. This reminds us that detection of a component present at the ppm level of concentration is not automatically equal to a tiny amount of sample.

Obviously, SS-MS is not suited for elemental analysis of small sample amounts, but SS-MS offers a high dynamic range making it very powerful for multiple element analysis including those present at trace level in alloys, ores, and similar samples. SS-MS also offers wide element coverage, an extensive concentration range and analysis of solids without dissolution.

The spark is initiated by emission of electrons from the cathode by field emission (opposite process to FI), which becomes possible due to the high local field strengths (10^8–10^9 V m^{-1}) at edges of the microscopically rough surface. The electrons are then accelerated towards the anode. There, the energy of the impinging electrons causes evaporation of the anode material (sample) that is subsequently ionized in the gas phase by electron ionization.

Proper operation of a spark source is not simple. It requires a high voltage supply of several tens of kilovolts, normally at 1 MHz radiofrequency that is generated in short pulses of variable length (20–200 μs) with a repetition frequency of 1–10^4 s^{-1} to achieve uniform ablation of both electrodes (Fig. 15.6) [44]. In order to maintain a stable ion current, the electrodes need to be carefully adjusted and dynamically re-adjusted during the measurement (0.1–0.5 mm tip to tip) [46], and special techniques such as *gliding spark source mass spectrometry* (GSS-MS) are sometimes employed for the analysis of nonconducting materials [47]. Finally, the ions emerge from the discharge with a wide kinetic energy distribution (keV range), which makes a double-focusing mass analyzer mandatory for SS-MS. To partially

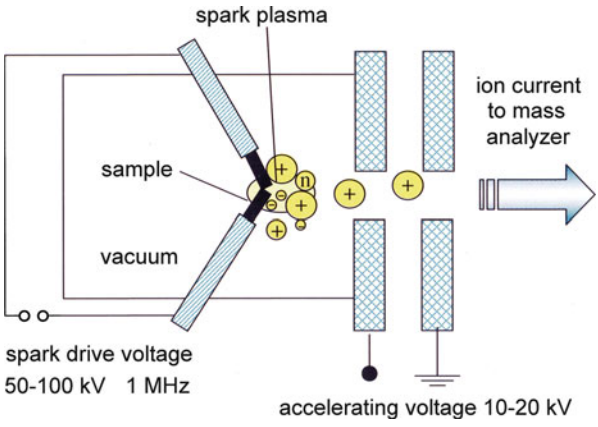

Fig. 15.6 RF spark source (Reproduced from Ref. [7] with permission. © John Wiley & Sons Ltd., 2008)

compensate for this high energy spread, accelerating voltages on the order of 20–25 kV are typical.

Opposed to all other current MS techniques, photoplate detection and subsequent densiometry on a series of exposures is still widespread in SS-MS. In practice, 15 consecutive spectra are acquired by exposing the plate streak-by-streak in a range from 0.001 to 300–2000 nCi, requiring total measurement times of about 0.5–3 h per sample. Translation of densiometric data into ion abundances is not trivial and detailed procedures have been developed for this crucial step of SS-MS analysis [43–45]. More recently, *multi-ion counting* (MIC) systems have been due to their improved sensitivity, precision, and sample throughput [45, 46]. Simultaneous detection in Mattauch-Herzog geometry SS-MS instruments using MIC is also advantageous for applications such as isotope dilution analysis of several isotopes. Furthermore, SS-MS is well suited for C, N, O determination in semiconductors, because the combination of a high vacuum source without sputter gas with a high frequency discharge allows for the analysis of samples even those of resistivities [48].

Carbon in gallium arsenide SS-MS has been used for the quantification of carbon in a gallium arsenide (GaAs) sample produced by high-pressure liquid-encapsulated Czochralski (HP-LEC) crystal growth. The carbon might originate from the graphite susceptor, the ambient gas, or be present as a trace element in both gallium and arsenic starting material. The partial SS mass spectrum shows strong signals due to $^{69}Ga^{6+}$, $^{71}Ga^{6+}$, and $^{75}As^{6+}$ in close proximity to the carbon peak at m/z 12 (Fig. 15.7) [49].

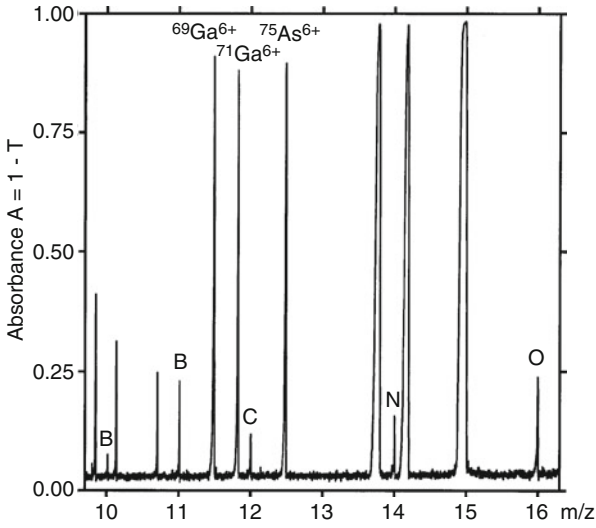

Fig. 15.7 Partial SS mass spectrum of a HP-LEC GdAs sample by photoplate detection after exposure to $Q = 3 \times 10^{-7}$ Ci Reproduced from Ref. [49] with permission. © Springer-Verlag, 1999)

15.4 Glow Discharge Mass Spectrometry

The first report of the formation of positive ions of gases from a *glow discharge* (GD) in his so-called channel ray tube was by Goldstein in 1886 [7]. Since the launch of the first commercial instrument for *glow discharge mass spectrometry* (GD-MS) in 1984, GD-MS has become sort of industry standard for the analysis of trace elements in metals and semiconductors [50, 51]. The pioneering work and much of the development of GD-MS has been done by Harrison and Marcus [52–56]. In fact, GD-MS appears as the successor to SS-MS, and at present, GD-MS is one of the most powerful solid-state analytical methods for the determination of trace impurities and depth profiling of solids. It allows direct trace element determination in solids down to concentrations as low as 1 ppb (ng g^{-1}) [32]. GD-MS is an essential technique for the quality control and characterization of high-purity metals in the electronics industry [57, 58].

The direct current (DC) glow discharge is a self-sustaining low pressure gas discharge dominated by space charges and represents a low-energy plasma making the GD ion source a compact small volume source that operates a low wattage. It is inexpensive to build and maintain, and plasma gases are modestly consumed (ml min^{-1}). Also, unlike the spark source, the GD source is inherently stable [59]. Typically, in a GD ion source [48, 51, 59–63] a discharge current of 1–5 mA is maintained through a low-pressure argon atmosphere (10^1–10^3 Pa) by applying a DC voltage of 500–2000 V across the ionization volume. The cathode is represented by the solid sample which may either be a disk (so-called *Grimm-type GD source* [59]) or a stick and an anode present as the housing and the ion source exit plate (Sect. 5.3 in [6], Sect. 7.5 in [3]).

The low-temperature Ar plasma serves as a source of primary ions, excited atoms and electrons. In the cathode dark space, a region where a large potential drop exists, the positive argon ions are accelerated towards the sample cathode and the sample material is sputtered from the cathode's surface by ion bombardment (cf. FAB, LSIMS, Chap. 10). The kinetic energies of the impinging ions are in the range of 100–500 eV [51]. Sputtered atoms and molecules depart from the surface with kinetic energies of 5–15 eV and are then ionized in the quasineutral glow discharge plasma (so-called *afterglow*). The electron density in the plasma can reach up to 10^{14} cm^{-3} [64] and their energy covers a wide distribution from thermal to energetic. Although they are by about a factor of 1000 less abundant in the plasma, metastable Ar* atoms are also effective for ionization because they carry 11.55 eV. Therefore, Penning ionization, electron ionization, and charge transfer contribute to ionize the neutrals (Fig. 15.8).

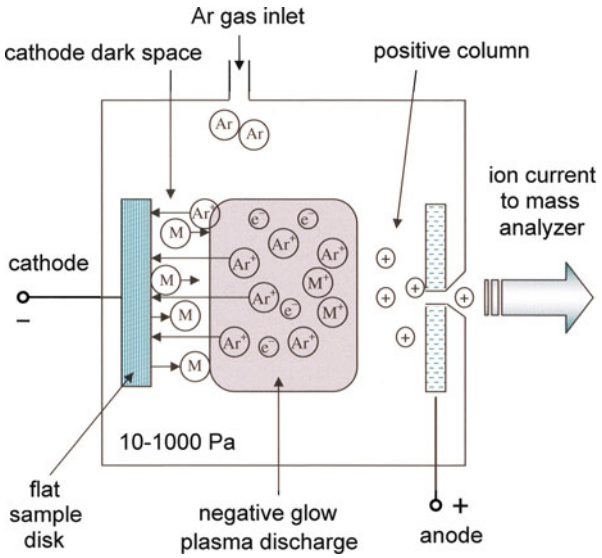

Fig. 15.8 GD ion source with disk-shaped cathode (Reproduced from Ref. [7] with permission. © John Wiley & Sons Ltd., 2008)

Shining brightly
The afterglow (or negative-glow) region shines brightly because excited atoms are emitting their characteristic visible radiation. This phenomenon not only gave rise to the method's name but also led to the construction of the neon lamp. For more applications of GDs a review by A. Bogearts is highly recommended [65].

Due to its general setup, GD has the advantage that the atomization and ionization processes are separated in space and time, resulting in only minor variations in sensitivity and a low matrix dependence. This enables the quantification of elements without the need for standards tailored to the actual type of sample matrix [48, 51].

On the downside, there are isobaric interferences such as $[XAr]^{+\bullet}$ and $[XH]^{+}$ ions that require $R > 5000$ to avoid overlap with pure atomic ions $X^{+\bullet}$ [51]. Therefore, double-focusing magnetic sector instruments present the most successful mass analyzers in GD-MS [48]. Another disadvantage of GD-MS as compared to LA-ICP-MS or SIMS (Sects. 15.4 and 15.5), for example, is the lack of spatial resolution.

Quality control of superalloy In the manufacture of aircraft engines and gas turbines superalloy is widely used due to its excellent performance, which to a great extent depends on the content of trace elements in the alloy. Critical control of the alloy's composition is therefore essential for the safe operation of such

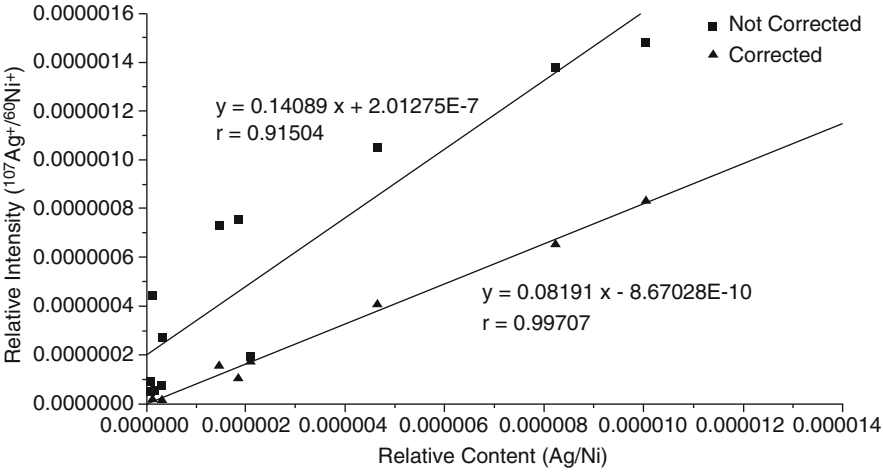

Fig. 15.9 Comparision of ^{107}Ag calibration curves in superalloy between the uncorrected results and those corrected by multivariable linear regression. The relevance of corrections when no separation by high-resolution is available is immediately apparent (Adapted from Ref. [66] with permission. © IM Publications, 2008)

engines. The obvious method to avoid isobaric interferences is to select isotopes where no interferences exist. While Tl, Pb, and Bi meet this criterion, in case of Sn only the $^{118}Sn^{+\bullet}$ ion is free of superimpositions, whereas $^{120}Sn^{+\bullet}$ has serious interferences from $^{40}Ar_3^{+\bullet}$, $^{92}Mo^{14}N_2^{+\bullet}$, and $^{120}Te^{+\bullet}$. To determine the correct content of elements in superalloy on a quadrupole GD instrument also when no suitable isotope exists, both matching the sample matrix by use of external standards and multivariable linear regression have extensively been used (Fig. 15.9) [66].

In a DC GD, nonconducting samples would rapidly cause the breakdown of the discharge due to electrostatic charging. Radiofrequency (RF) discharges circumvent this problem [54–56, 61, 67]. By applying an RF voltage at one of the two electrodes (called the *RF-electrode*), the accumulated positive charge on the sample surface will be neutralized by the negative charge accumulation during the second part of the RF-cycle thereby avoiding net charges. Typically voltages of 2 kV at an RF of 13 MHz are employed.

The atomic collision processes in the GD are sufficiently robust to break many tenaciously bonded species [59]. Nonetheless, GC-GD-TOF-MS has even been demonstrated to be capable of delivering spectra of organic molecules and elemental information [68–70].

Need to zoom in

The analytical problems of inorganic MS often require only certain selected isotopes or narrow m/z ranges to be measured. Multicollector systems, for example, are adjusted to simultaneously detect a few isotopes for the purpose of accurate isotope ratio determinations or to quantify a low-abundant isotope together with an isotopic standard for internal reference. Thus, the data is more often presented in tabular form or in plots of concentration versus variables such as depth of invasion, age of samples, or location on a surface. Mass spectra covering a wider range are only acquired for survey multi-element detection.

15.5 Inductively Coupled Plasma Mass Spectrometry

In *inductively coupled plasma mass spectrometry* (ICP-MS), atomization and ionization are achieved in a radiofrequency argon plasma at atmospheric pressure. Since a seminal publication in 1980 [21], ICP-MS has become one of the most frequently employed methods of elemental MS ([57, 58], Sect. 7.3 in [3], Chap. 4 in [6], Sect. 5 in [7]). The wide acceptance of ICP-MS is due to its comparatively robust, yet versatile sampling mode. An ICP not only offers high ionization efficiency for elements of low *IE*, e.g., 98% for $IE = 7$ eV, it is still applicable to nonmetals such as P and even Cl (ionization efficiency is 1% for $IE = 13$ eV).

The core of an ICP source is formed by a so-called *plasma torch*. It consists of three coaxially aligned quartz tubes that are inserted along the central axis of a water-cooled RF coil. After ignition by an electric spark discharge, the coil (typically RF of 27 MHz) feeds the plasma by coupling electric energy (1–2 kW) into the gas, because the fluctuating magnetic field causes ion motion which in turn heats up the gas and maintains a continuously flowing plasma. The outer quartz tube is about 20 mm in diameter and has its walls cooled by an argon gas flow of 12–20 l min^{-1}. The middle tube supplies another stream of argon, the so-called auxiliary gas flow of 1–2 l min^{-1} that is feeding the plasma. The sample is then introduced into the center of the toroidal plasma by an argon carrier gas flow of 1–1.5 l min^{-1}. This carrier gas passes through a nebulizer and leads to the dissipation and transfer of a liquid sample as micrometer-sized droplets (depending on the type of nebulizer), which can be vaporized, atomized, and ionized within the ICP. Typical sample consumption is in the order of 0.02–1 ml min^{-1} (Fig. 15.10).

The ICP approaches a temperature of 10,000 K in the induction zone close to the coil, in the center of which evaporation and atomization occur at about 8000 K. While the plasma flows away from the coil, excitation of the neutrals is effected at 7500 K followed by ionization in a zone well after the coil at about 6000 K (Fig. 15.10). Thereafter, recombination in the plasma's tail causes molecular interferences, which can be reduced by placing a collision cell in the ion beam, for example [30, 31, 72, 73].

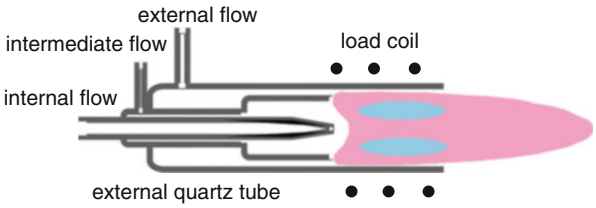

Fig. 15.10 ICP torch. Three concentric quartz tubes deliver the internal flow containing the sample, the intermediate argon flow to support the plasma, and an external flow to provide cooling to the outer wall. The temperature reaches about 10,000 K inside the coil and drops to about 6000 K at the tip of the plasma from where ions are collected at the sampling cone (Adapted from Ref. [71] with permission. © Royal Chemical Society, 2015)

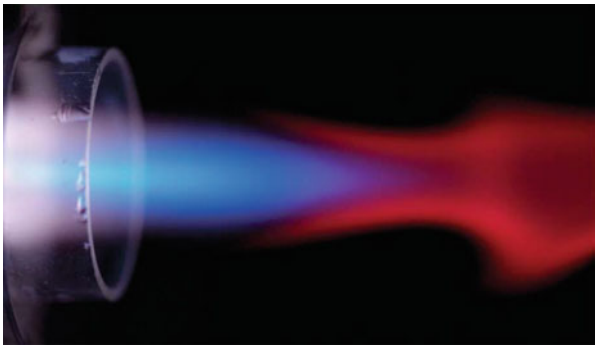

Fig. 15.11 ICP plasmas can be beautiful. This photograph shows a plasma as obtained during the analysis of yttrium (Reproduced from Ref. [74] with permission. © Royal Chemical Society, 2003)

The appearance of the plasma varies and depends on liquid and gas flow, nebulizer design, and of course, the type and concentration of the analyte. In some cases, the ICP can be extraordinarily beautiful (Fig. 15.11) [74]. Careful observation of the ICP by high-speed photography can reveal carryover of particles from laser ablation (LA) or of droplets into the ICP due to overly high liquid flow [74].

Analogous to ESI (Chap. 12), ion transfer into the mass analyzer is accomplished via a differentially pumped interface. A small portion of the plasma enters the first pumping stage through a hole in the center of the sampling cone. Water cooling of the sampling cone preserves its surface from rapid destruction due to the exposure to the hot plasma. Next, the ions are guided through the entrance of the skimmer by application of an electric potential, while most neutrals are pumped off the supersonic expansion in this region (Fig. 15.12). Analogous to early atmospheric pressure ion sources of organic MS, the first implementation of ICP-MS was attached to a quadrupole analyzer due to its acceptance of moderate vacuum conditions [21].

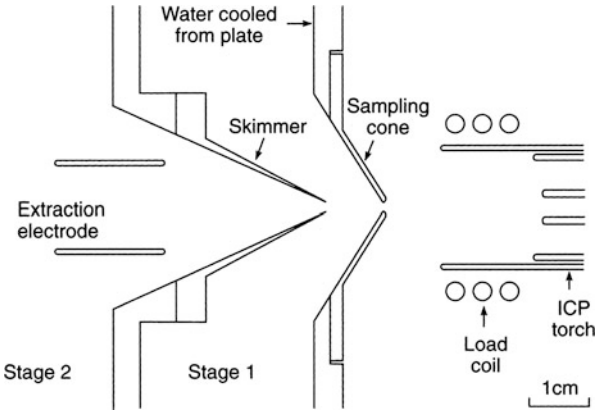

Fig. 15.12 Ion extraction interface for ICP-MS. Ions arrive from the right, a small portion is transmitted through the water-cooled sampling cone into the first pumping stage (rotary pump), the center of the free-jet expansion is then transmitted through the second skimmer cone, behind which it is guided by electric potentials through the second pumping stage (turbo pump) into the mass analyzer (Reprinted with permission from Ref. [3]. © John Wiley & Sons Ltd., 1997)

Nowadays, ICP sources are used with magnetic sector [13, 75], to an important extent time-of-flight (TOF) [76–81], and even Fourier transform ion cyclotron resonance (FT-ICR) mass analyzers [82].

The interest in high-resolution ICP instruments is driven by polyatomic interferences between the plasma gas and the matrix introduced, which are indeed limiting factors for ICP-QMS. Isobaric interferences are less problematic than it might appear on first sight, since most of the elements have more than two isotopes to select from. Anyway, none of the isobaric interferences can be resolved by the current sector or TOF mass spectrometers since they require a mass resolution above 12,000 [83].

Multicollector detection systems are an important feature of element MS instrumentation as simultaneous detection of all ions of interest provides the most accurate isotope ratios [84, 85]. The traditional approach employs multiple Faraday cups that can be adjusted along a sophisticated rail to collect a set of ions. A more recent ICP mass spectrometer allows ions along the 120-mm focal plane of a small Mattauch-Herzog geometry analyzer to be detected simultaneously. This is accomplished by use of a large direct charge semiconductor detector that provides 4800 channels covering the focal plane. Thus, 210 nuclides from ^{6}Li to ^{238}U can be monitored without scanning, i.e., at constant magnetic field [85]. The particular ICP mass spectrometer even relies on a permanent magnet and its ion optical path is complemented by a 127° electrostatic sector as pre-filter in front of the Mattauch-Herzog analyzer in order to prevent photons and neutrals from the ICP from entering the actual mass analyzer.

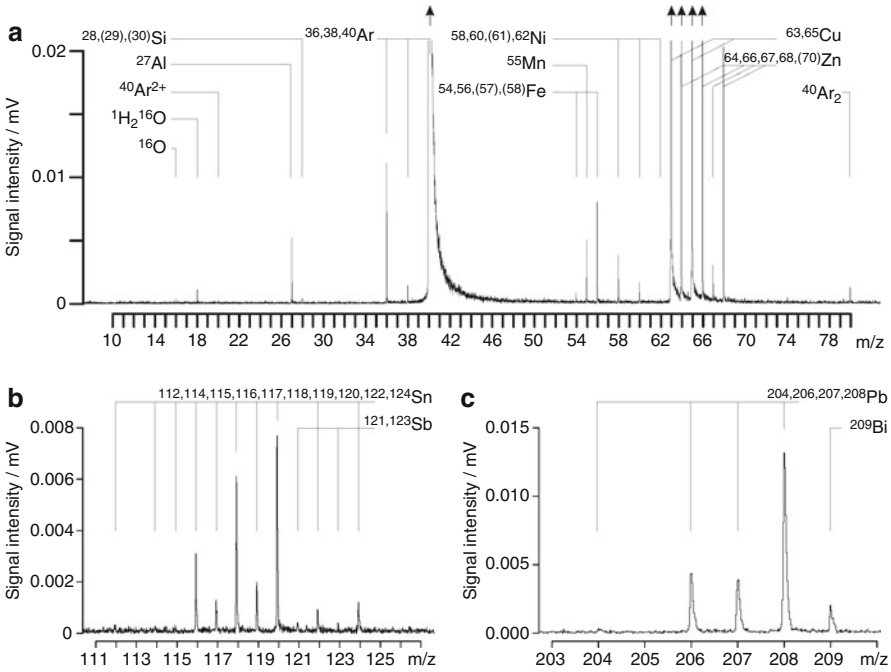

Fig. 15.13 The ICP-TOF mass spectrum of brass. The peaks due to N, O, H_2O, Ar^{2+}, Ar^+, and Ar_2^+ are present as a blank spectrum of the ICP. In range (**a**) up to *m*/*z* 80, Si, Mn, Fe, and Ni are detected at low levels while Cu and Zn are dominant as expected for brass. The sections (**b**) and (**c**) show overlapping signals from Sn and Sb as well as Pb and Bi, respectively (Adapted from Ref. [81] with permission. © Springer-Verlag, 2008)

Distinguished acronyms

In inorganic mass spectrometry, the type of mass analyzer occasionally becomes part of the acronym: a quadrupole leads to ICP-QMS, a magnetic sector field leads to ICP-SFMS, and use of a double-focusing analyzer may be indicated by ICP-DFMS, respectively. Thus, a time-of-flight analyzer attached to an ICP source would be referred to as ICP-TOFMS. Again, this is slightly different from the customs in organic and biomedical mass spectrometry where only TOF and FT-ICR tend to be included in the acronym and normally are separated by a hyphen from MS.

Liquid sample introduction is still the standard in ICP-MS. Consequently, the coupling of liquid chromatography or capillary electrophoresis to ICP instruments is straightforward. This way, not only the presence of an element in a sample can be detected, but also the assignment to molecular species becomes feasible. This explains the relevance of ICP-MS for the identification of non-C,H,N,O elements in proteins, i.e., for metallomics (cf. first two examples of this chapter).

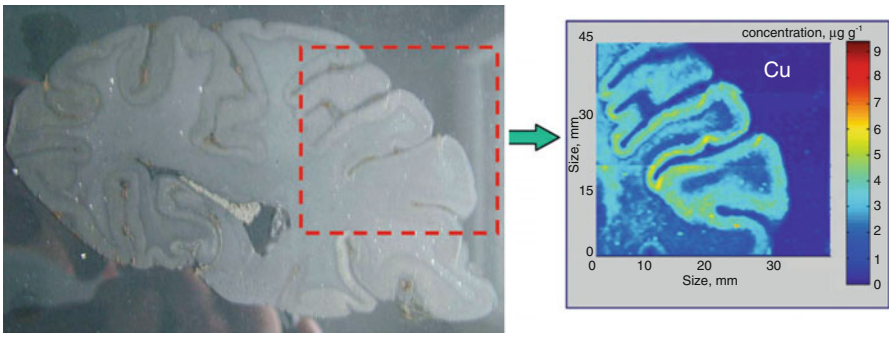

Fig. 15.14 Mass spectral imaging to unveil the quantitative distribution of Cu in tissue. The average concentration of Cu was 3–7 µg g^{-1} tissue. Light photograph of a thin tissue section of human brain (*left*) and the Cu distribution in the marked region as obtained by LA-ICP-MS (*right*) (Adapted from Ref. [18] with permission. © The Royal Society of Chemistry, 2007)

ICP-TOFMS of brass Three categories of signals are contributing to the ICP mass spectrum of brass. The background peaks due to $^{14}N^+$, $^{16}O^+$, $^1H_2{}^{16}O^{+\bullet}$, $^{40}Ar^{2+}$, $^{36,38,40}Ar^+$, and $^{40}Ar_2{}^+$ are contributions of the ICP background spectrum. Then, the polyisotopic elements Cu and Zn represent the main components of brass, and thus, cause strong peaks. Finally, Si, Mn, Fe, Ni, Sn, Sb, Pb, and Bi are present at low concentration (Fig. 15.13). Instead of nebulizing a solution of the alloy, in this particular case the brass has been fed into the ICP by in-torch laser ablation [81].

Need for sample preparation
ICP-MS is commonly mentioned in the context of high throughput and claimed to have no need for extensive sample preparation. In analytical practice, however, every sample needs to be treated individually; digestion prior to analysis usually takes about 2 h per sample. Furthermore, as is the case with TIMS for example, matrix separation is required for precise and accurate isotope ratio determinations. In particular, if MC-ICP-MS is going to be used as a complementary technique for TIMS, high throughput is only achieved on the expense of precision.

15.5.1 Laser Ablation ICP-MS

To further complement the sampling repertoire for ICP-MS, a gas stream, typically helium, may be employed to take up a laser-generated aerosol. This technique is known as *laser ablation* (LA) ICP-MS. Its first realization by the Hieftje group in

1996 [86] was based on the previously introduced ICP-TOF instrumentation [76–78]. LA-ICP-TOF-MS can be used for sampling from solid surfaces of bulk material, or alternatively, for imaging of element distributions. LA-ICP mass spectral imaging allows to monitor the lateral distribution of elements across a solid structure [87], to identify metals and metalloids on a 2D gel [88, 89], or to reveal element concentrations in biological tissues and similar samples (Fig. 15.14) [17, 18, 20, 89, 90].

15.6 Secondary Ion Mass Spectrometry

When a beam of (primary) ions possessing keV-energies strikes a surface, the energy transferred by the incident particles causes a collision cascade that sets several atomic layers in motion and is accompanied by complex processes of energy transfer and electronic interaction in the surface zone of the solid. It results in the emission of electrons, photons, atoms, and molecules, both of the latter either neutral or ionic, whereby the surface under bombardment experiences irreversible changes [91]. The ions that are emitted are termed *secondary ions* and the method is therefore called *secondary ion mass spectrometry* (SIMS). Nearly the same processes of sputtering and ion formation are effective in FAB and LSIMS (Chap. 10) [92], and in fact, SIMS paved the road for the development of FAB and LSIMS to analyze organic samples. Nonetheless, SIMS is not simply a precursor of FAB, but a reputable method of its own serving nicely for analyzing inorganic samples that range from rocks to alloys and semiconductors [93, 94].

The emission of secondary ions of both polarities from instrument construction materials produced as a by-product of ion source operation was first observed by Arnot [95, 96] and was developed into an analytical instrument by Herzog and Vieböck [97]. Inspired by these experiments, an early SIMS instrument was constructed in the 1960s to analyze lunar rocks from NASA's Apollo missions. Much of the breakthrough of SIMS for *i)* bulk analysis of solids, *ii)* depth profiling of thin layers, *iii)* imaging at high lateral resolution, and *iv)* monolayer analysis is also the merit of the Benninghoven group [91, 93, 98, 99].

15.6.1 Atomic SIMS

Applied to solid materials, especially semiconductors and thin films, SIMS can determine trace levels of all elements in the periodic table. Spatial microanalysis is provided by collimating the primary ion beam to about 1 μm in diameter and control of where the beam strikes the sample surface. This way, SIMS provides lateral and depth distributions of these elements within the sample. Currently, SIMS is being adapted to achieve lateral resolutions well below 100 nm. The driving force comes from the progress in microelectronics aiming at structures that approach 10 nm. Also, the depth resolution needs to come close to the atomic scale [100].

SIMS surface analysis is classified into two modes of operation, the so-called *static SIMS* and *dynamic SIMS* mode.

Static SIMS employs an extremely low sputtering rate, often with a pulsed primary ion beam, for better sensibility to the characteristics of the top monolayer and even may reveal molecular information (see below) [101]. In static SIMS, the primary ion dose is kept below 10^{12} ions s^{-1} cm^{-2}.

Dynamic SIMS uses high sputtering rates of a constant primary ion beam (10^{17} ions s^{-1} cm^{-2}) resulting in very high sensitivities to trace impurities (ppm to ppb). It delivers elemental and isotopic information as do the other methods of inorganic mass spectrometry. Magnetic sector or quadrupole mass analyzers are frequently in use for dynamic SIMS. Continuous analysis while sputtering yields information as a function of depth, called a *depth profile*.

Each impact an event of its own

A single sputtering event, i.e., penetration, lattice perturbation by impact cascades, and final particle ejection, takes less than 10^{-12} s. Interestingly, for primary ion beam densities $<10^{-6}$ A cm^{-2} (equal to 6×10^{12} ion s^{-1} cm^{-2}) no interference of processes caused by different primary ions will occur, because the maximum cross section of an impact is only in the order of 10 nm^2. In other words, each impact is independent of prior, subsequent, or nearby synchroneous hits [91, 92]. In the time domain this means that a given surface area suffers 10–100 hits min^{-1} in dynamic SIMS, but only 0.01–0.1 hits min^{-1} in static SIMS. For a monoatomic layer, observation times in the order of 1 h can thus be realized in static SIMS, i.e., the attribute *static* refers to the extended preservation of the surface.

15.6.2 Instrumentation for Atomic SIMS

The primary ions for SIMS are usually generated by either a thermal ionization source delivering Cs^+ ions or by a *duoplasmatron source*. Depending on its mode of operation, the duoplasmatron is working somewhere between electron ionization and a glow discharge. It can be used to generate a collimated beam of positive (Ar^+, O^+) as well as negative primary ions ($O_2^{-\bullet}$) [102, 103]. Positive oxygen ion bombardment increases the concentration of oxygen in the surface layer and creates M–O bonds there. Breaking these bonds during the process of bombardment and ion desorption builds up negative charge that is readily consumed by the oxygen because of its high electron affinity. Thus, more metal atoms remain positively charged. Strongly electropositive elements are therefore analyzed as positive secondary ions from oxygen bombardment for best sensitivity. Opposed to oxygen, cesium ions implanted into the sample surface reduce its work function, thereby providing more secondary electrons, which enable effective negative ion formation.

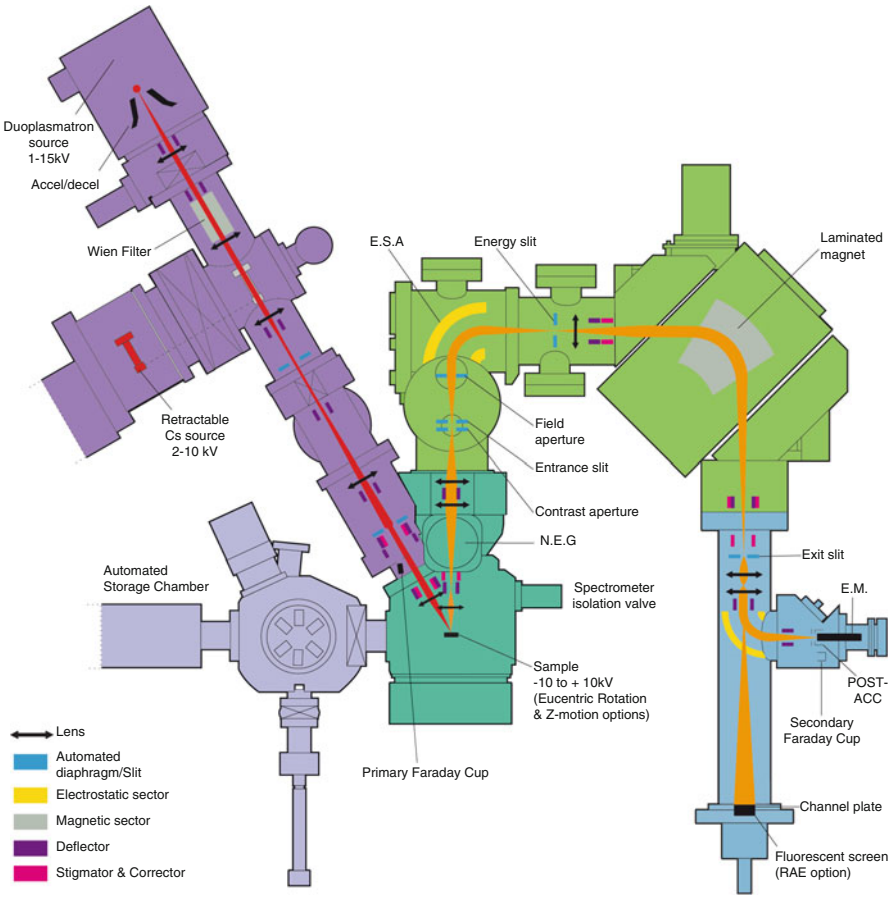

Fig. 15.15 Schematic of the CAMECA IMS 7f-Auto showing the main components of a high-resolution ion microprobe SIMS instrument. For flexibility the sample can be bombarded with either Cs^+ ions (by TI) or ions from a duoplasmatron source, which can deliver noble gas or oxygen ions. The double-focusing magnetic sector instrument of EB geometry offers high resolution and ion detection by either SEM, Faraday cup, or MCP (Reproduced from CAMECA technical literature with kind permission. © CAMECA Germany, 2016)

Consequently, semimetals and nonmetals as well as group VIII transition metals are preferably analyzed by Cs^+ bombardment as negative ions.

Another well-established class of primary ion sources are *liquid metal ion guns* (LMIG) delivering Ga^+ or In^+ ions. They offer very fine beams to achieve high lateral resolution. The Ga^+ LMIG currently provides the smallest probe size (less than 10 nm) with the highest current density (1–10 A cm^{-2}) of any ion gun. The LMIG normally consists of a field emitter tip coated with Ga from where a high electric field extracts Ga^+ ions. To ensure optimal focusing of the beam, the Ga^+ ions are accelerated by 20–60 kV (Fig. 15.15) [104].

Sputtering as a result of primary ion bombardment delivers diverse ion species ranging from monoatomic ions of various charge states to multi-atomic clusters and eventually simple molecular ions. Sputtering is generally accompanied by isotopic and chemical fractionation, i.e., the secondary ion yield is not independent of the material to be analyzed. SIMS produces spectra that are characterized by numerous interferences between different charge states of atomic ions and simple reaction products such as oxides, hydroxides, halides, etc. As with any other elemental MS technique before, high-resolution instruments provide the most effective and reliable means of dealing with superimposing isobars.

Ions generated by SIMS The positive secondary ion spectrum of a silicon surface shows peaks that can be assigned to Si^{2+}, Si^{+}, Si_2^{+}, Si_3^{+}, Si_4^{+}, etc. while the negative secondary ion spectrum yields signals corresponding to Si^{-}, Si_2^{-}, Si_3^{-}, and Si_4^{-}. In case of a two-component lattice such as a metal (M) oxide, SIMS will deliver positive ions of the type $[M_nO_{n-1}]^{x+}$ (normally $x = 1$) and negative ions of the general type $[M_{n-1}O_n]^{-}$. The number ratios of M and O will naturally depend on the metals' prevailing oxidation state. Accordingly, more complex systems result in additional cluster ion compositions. SIMS of salts preferably yields the cation or anion and corresponding cluster ion series as already mentioned for FD, FAB, or ESI (Chaps. 8, 10, and 12, respectively) [91, 98, 99].

15.6.3 Molecular SIMS

Static SIMS, i.e., conditions of low primary ion flux, can preserve molecular information, but this is effected at the expense of correspondingly low secondary ion yields. The combination of static SIMS conditions with scanning mass analyzers is therefore disadvantageous and the outcome of experiments with SIMS for organic molecules such as amino acids in the "pre-FAB era" was not too exciting [101]. Here again, the TOF analyzer plays to its strength as it is capable of analyzing all ions contained in a package created by a short primary ion pulse. As only few ions are lost (due to imperfect transmission) there is a more than 1000-fold gain in sensitivity when using a TOF rather than a quadrupole analyzer [105].

The first TOF-SIMS instrument [106] employed a pulsed alkali primary ion source. The primary ions were created from alkali aluminosilicate by thermionic emission, accelerated by up to 25 keV and focused onto the monomolecular sample layer on gold or silver surfaces in bursts of 5–50 ns. (This type of Cs^{+} primary ion sources is still in use for LSIMS.) Useful spectra of amino acids and nucleosides [106, 107] and even peptides [108] were obtained in this way. Soon, TOF-SIMS became a major competitor of PD-MS [109–111] and the development of FAB and LSIMS led to fruitful approaches such as TOF-LSIMS [112].

Modern TOF-SIMS applications are often in the field of synthetic polymer analysis, but rarely for the determination of molecular weight distributions which is the domain of MALDI. More frequently, low-molecular-weight additives or surface modifications are analyzed as there is no interference with a matrix as

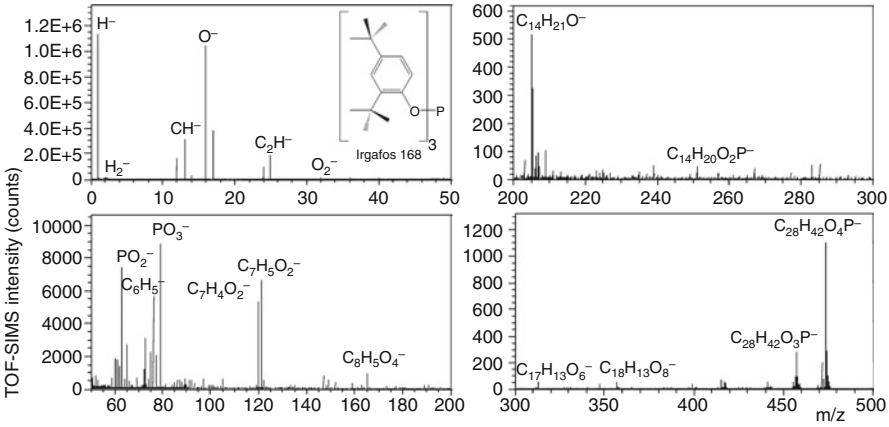

Fig. 15.16 Negative-ion TOF-SIMS analysis of Irgafos 168 on PETi. The compound undergoes significant fragmentation, and thus, no $[M–H]^-$ peak (m/z 645) is included. Note the tremendously decreasing ion abundances with rising m/z, which is also the reason for the segmented representation of the mass spectrum (Reproduced from Ref. [117] with permission. © John Wiley & Sons, Ltd., 2002)

would be the case with MALDI [113–117]. In essence, only SIMS can truly analyze the native surface.

Polymer additives by SIMS Additives are intentionally added to a polymer to stabilize or improve different polymer properties. They act as antioxidants, UV stabilizers, antistatic agents, flame retardants, etc. However, their migration towards the surface may result in blooming, thereby negatively affecting surface properties that are required for specific applications. TOF-SIMS is ideally suited to characterize surface compositions because it offers molecular information on the uppermost monolayers at high sensitivity. Here, the antioxidant Irgafos 168 (0.3 wt.%) has been analyzed on the copolymer PETi, a poly(ethylene terephthalate (60%) isophthalate (40%)) (Fig. 15.16) [117].

15.6.4 Polyatomic Primary Ion Beams

More recently, SIMS has gained enormous impetus from the introduction of heavy primary ion beams such as gold [118] or bismuth clusters [119–121] or fullerene molecular ions [27, 122–124]. Especially their combination with TOF-SIMS instrumentation has rejuvenated the whole field of SIMS. As we already know from FAB and LSIMS, and as has been veryfied also for SIMS [125], higher-mass xenon beams create a higher yield of secondary ions and are more effective for larger molecules than argon or neon, for example. Before the advent of heavy primary ion sources, the ions which could be detected by TOF-SIMS were limited to a mass range of about 300 u mainly because the primary ions where very inefficient in

desorbing larger molecular species. With polyatomic primary ion beams the secondary ion emission is drastically enhanced while the surface damage is not as severe [126]. Polyatomic primary ion beams can effectively cover the range up to m/z 1500 at lateral resolutions in the order of 1 μm.

Experiments and molecular dynamics theory suggest that the efficient ionization of large molecular species requires the concerted action of a number of collision cascades. Atomic primary particles focus the energy deposition in a very small area but quite deep into the solid. Polyatomic primary ions, on the other side, break apart upon collision with the surface, this way creating numerous weaker impacts over a wider range [123]. The concerted action of a number of soft impacts can effect the desorption of the molecule [105]. Molecular dynamics simulations suggest that an acoustic wave is generated that essentially pushes the secondary ions off the surface. Especially fullerene ion sources ($C_{60}^{+\bullet}$ primary ions [105]) lead to energy deposition in the uppermost sample layers.

Surfactins from *Bacillus subtilis* Even with the advent of cluster ion sources, TOF-SIMS imaging favors hydrophobic molecules. Surfactins are a family of heptacyclodepsipeptides where the C-terminal carbonyl is linked with the β-hydroxy group of a fatty acid that is acylating the N-terminal function of a glutamic acid residue. The fatty acyl chain is 12–16 carbon atoms long. These compounds are secreted by the Gram-positive bacterium *Bacillus subtilis* and play an important role in the formation of dendritic patterns. Mapping of these surfactins by TOF–SIMS imaging showed that they were mainly located in the central mother colony, in a 'ring' surrounding the pattern and along the edges of the dendrites (Fig. 15.17). Surfactins with shorter chain lengths are found in the interior of the dendrites, whereas surfactins with longer fatty acyl chain lengths were found in the ring surrounding the swarm community [126].

Data handling and storage
Mass spectral imaging creates sort of a "chemical map" filled with enormous amounts of data. A standard image of 256 × 256 pixels requires 65,536 mass spectra each possessing about 10^5 data points. Therefore, effective software tools for data evaluation, representation, and eventually compression for long-term storage are necessary to deal with those gigabytes of data.

The future for SIMS seems bright and promising. From a seemingly disappearing technology at the very beginning of this millennium [27], it has stood up to deliver impressing results such as the imaging of bones, tissues, and even single cells [25, 27, 121, 123, 127, 128]. Advanced sample preparation techniques such as cryofreezing of tissues open up the new capabilities of holding these samples under low vacuum conditions for the time span of the experiment.

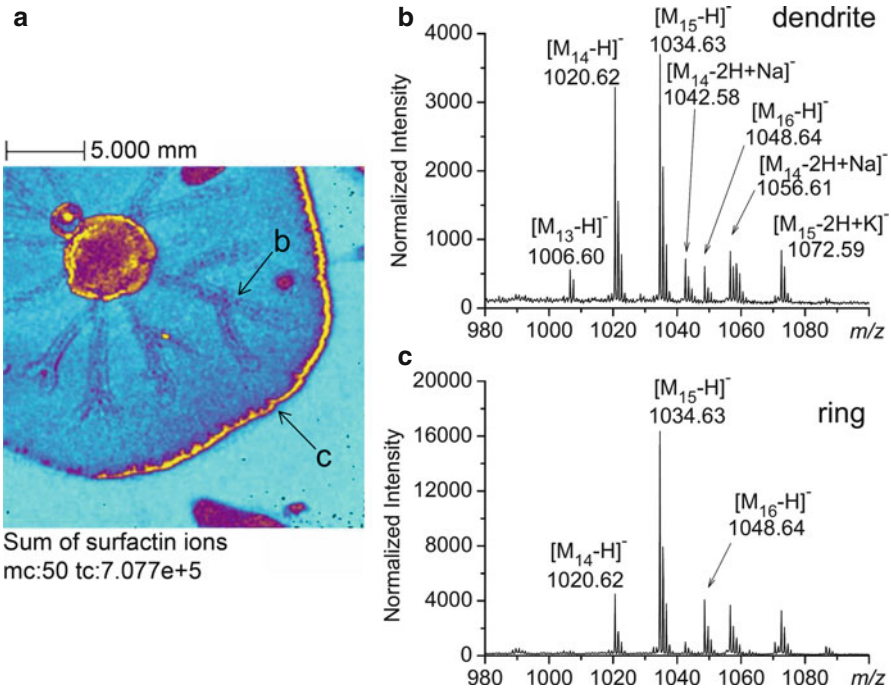

Fig. 15.17 (**a**) TOF-SIMS image of the sum of surfactin ions at the surface of a *Bacillus subtilis* swarming community. The maximal number of counts in a pixel (mc) and the total number of counts (tc) are indicated below the image. Field of view 23 × 23 mm^2, 256 × 256 pixels, pixel size 90 μm, Bi_3^+ primary ion fluence 1×10^9 ions cm^{-2}. (**b**) Partial mass spectrum obtained from a region of interest drawn around a dendrite. (**c**) Partial mass spectrum obtained from a region of interest drawn around the ring. M_n refers to compounds possessing an alkyl chain being n carbon atoms long (Adapted from Ref. [126] with permission. © Springer-Verlag 2009)

Recently, MALDI and SIMS imaging are seen as complementary techniques to assess complex biological systems [26]. While MALDI can deliver information on peptides, proteins, oligosaccharides, and other high-mass constituents, TOF-SIMS is the tool of choice for the analysis of lipids, unaltered surfaces, and extremely fine structures [26, 28, 104, 124, 126]. The imaging community is now also using common instrumentation such as a SIMS/ESI/MALDI quadrupole-TOF instrument [129].

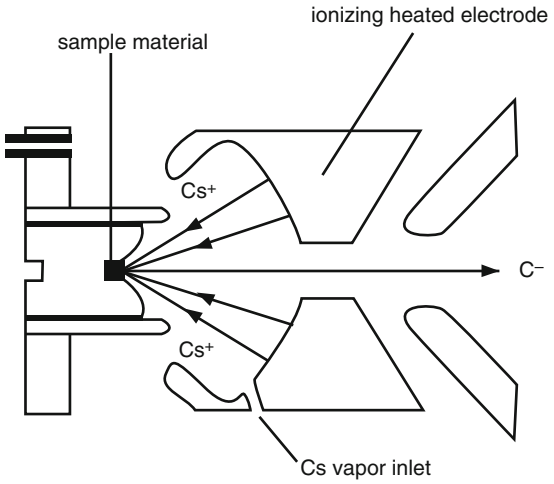

Fig. 15.18 High-intensity Cs sputter source for AMS. Cs^+ ions are created by thermal ionization of Cs vapor on a large heated tantalum anode that is placed over the sample like a dome. Secondary (analyte) ions exit through an axial aperture. Having the sample at negative high voltage accelerates the Cs^+ ions away from the anode to bombard the sample and also forces the analyte anions out of the source (Reproduced from Ref. [130] with permission. © Wiley Periodicals Inc., 2008)

15.7 Accelerator Mass Spectrometry

15.7.1 AMS Experimental Setup

The methodology of *accelerator mass spectrometry* (AMS) clearly differs from all other approaches to analyzing of atomic mass so far referred to in this book [4, 130]. While ions to be analyzed by a quadrupole analyzer are injected at kinetic energies of about 10 eV, those for a sector instrument at 5–10 keV, and those for TOFs at 15–30 keV, in AMS ions have several MeV. Another unique and key feature of the technique is that the ions experience dramatic changes in kinetic energy and charge state during the experiment.

To achieve this, the accelerator mass spectrometer consists of several stages. First, negative secondary ions of the sample are created by Cs^+ ion bombardment (Fig. 15.18). The primary step of mass analysis is conducted in a more-or-less conventional double-focusing magnetic sector unit. Mass-selected ions are then passed into a linear *Van de Graaff accelerator* or a *tandem accelerator*. These devices are frequent in nuclear physics. In a tandem accelerator, negative ions are attracted by high positive voltage, V_a, towards the high voltage terminal in the center of the vessel. An ion with z_1 elementary charges e has a charge $q = z_1 e$ and by the accelerator therefore receives an additional kinetic energy of $E_a = z_1 e V_a$. This ion is then passed through a so-called (charge) *stripper*. Two types of charge

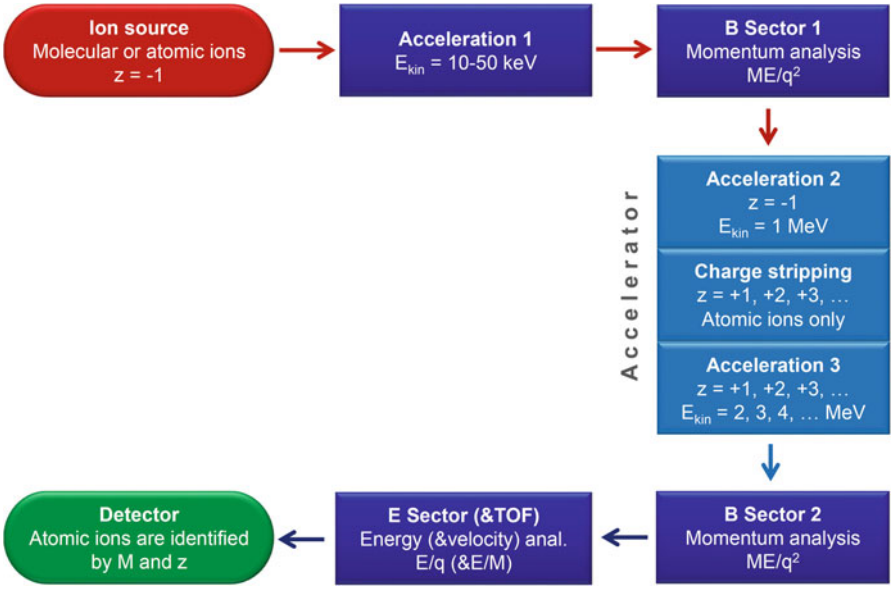

Fig. 15.19 Sequence of events and general experimental setup of AMS [4]. The instrument consists of a medium ion kinetic energy section, an ion accelerator, and a high-energy section to detect multiply charged atomic ions at highest sensitivity and specificity

stripping devices are in use: *i)* foil strippers, where the beam is shot through a thin carbon foil, and *ii)* gas strippers, essentially gas collision cells. Both serve to strip off all electrons from the anion, thereby converting it into a multiply charged positive ion, i.e., $q = -z_2e$. This extreme degree of charge inversion is the main purpose of the high collision energy – a very welcome side effect being the highly effective ion counting in the detector. The atomic cations are then pushed away from the high voltage terminal towards the exit of the accelerator on its opposite side. Due to their individual charge states the multiply charged positive ions gather different amounts of kinetic energy on the second stage of acceleration. After having passed the accelerator, the total kinetic energy received is given by $E_a = V_a \times (z_1e + z_2e)$. They are then separated according to their momentum, charge, and energy, and finally counted individually. This second unit also represents a sort of large magnetic sector instrument but it may have additional components such as a TOF analyzer for ion velocity analysis (Fig. 15.19) [4].

15.7.2 AMS Facilities

In particular, due to the accelerator, the classical AMS facility requires an area of some hundred square meters for instrumentation (Fig. 15.20). In recent years, the increasing demand for AMS measurements has led to the design of significantly smaller AMS instruments for dedicated purposes; this “miniaturization” has much

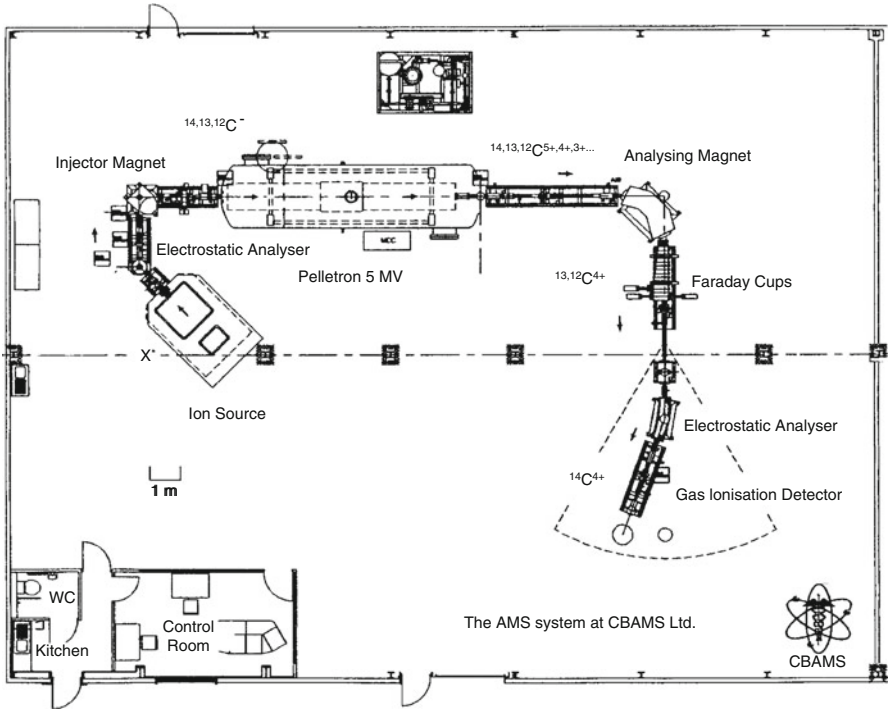

Fig. 15.20 AMS facility of CBAMS. The instrument is typical for its kind. Note the scale bar for 1 m. CBAMS, founded in 1997, is the first private company in the world to offer a fully commercial analytical service using an accelerator mass spectrometer (Reproduced from Ref. [14] with permission. © John Wiley & Sons, Ltd., 1999)

been driven by Suter in Zurich [131–133]. The concise review by Hellborg and Skog is recommended for further readings [130].

15.7.3 Applications of AMS

The great advantage of these MeV-energies is that they are able to help avoiding ambiguities in identification of atomic ions, because eventually interfering molecular species are completely destroyed at the stage of the charge stripper. Furthermore, selection of a suitable high charge state characteristic of the isotope to be analyzed allows to unequivocally identify the species. For example, the nuclei of ^{14}C, ^{26}Al, and ^{129}I are free of superimpositions from isobaric ^{14}N, ^{26}Mg, and ^{129}Xe, because the negative ions of the latter are unstable.

AMS is an extremely sensitive technique for isotopic analysis, in particular for measuring isotope ratios over an extreme dynamic range. For some elements such as carbon, isotope ratios of as low as 1 in 10^{15} can be determined. This is by a factor

of 10^5 lower than by any other MS technique [4]. Moreover, about 1 mg of sample is sufficient for AMS, which is equivalent to a content of only about 10^6 atoms of the isotope of interest. Thus, AMS is ideally suited for isotope ratio measurements of low-abundant isotopes, especially those having too long half-lives for determining radioactive decay from small sample amounts such as carbon-14. In fact, carbon-14 dating led to AMS [134, 135] and is still applied in various ways [14, 130, 136]. AMS is nowadays also employed for determination of isotopes such as ^{10}B, ^{26}Al, ^{36}Cl, ^{41}Ca, ^{129}I and others including stable isotopes. The versatility of AMS has led to impressing applications in the life sciences, geosciences, archeology, and extraterrestrial research [15, 19, 130, 137–139].

AMS wins over radioactive counting To illustrate the capabilities of AMS, we compare carbon-14 determination by radioactive counting to AMS. A sample of 1 g of environmental carbon contains 6×10^{10} atoms of ^{14}C (and 1.2×10^{12} times more ^{12}C atoms). Due to the 5730 years half-life of ^{14}C, only 13 atoms will decay per minute. For a statistical precision of 0.5% as normally required in radiocarbon dating, decays from 1 g of carbon need to be counted for more than 48 h. AMS does not have to wait for the decays, it is more efficient because it uses the whole sample. A sample of 1 mg carbon, only one thousandth of the material needed for decay counting, is completely sputtered in the ion source within 1–2 h and delivers about 6×10^5 atoms, which is 1% of the total ^{14}C content, to the AMS detector system. Conventional mass spectrometers cannot be used here, because the ^{14}C ions are superimposed by atomic and molecular isobars that are by orders of magnitude more abundant. These are $^{14}N^+$ and small fragments such as $^{13}CH^+$, $^{12}CH_2^{+\bullet}$, $^{12}CD^+$, and $^7Li_2^+$. Abundance sensitivity also plays a role by limiting the ^{14}C detection due to minor overlap with stretching peak bases from ^{12}C and ^{13}C. Conventional MS is therefore limited to isotope ratios of $^{14}C/^{12}C$ of approximately 10^{-7} at best. AMS achieves $^{14}C/^{12}C$ detection down to approximately 10^{-15}.

15.8 Summary

Concept of Inorganic Mass Spectrometry
Inorganic mass spectrometry or element mass spectrometry are collective terms for the field of MS aiming at the analysis of the elemental composition of a sample, the detection of trace elements or trace isotopes, and the determination of isotope ratios.

Instrumentation
Instrumentation of inorganic MS varies widely. It ranges from dedicated instruments in stable isotope ratio analysis to highly versatile secondary ion mass spectrometers that can be adapted to deliver the bulk composition of samples – even some molecular information – or even to provide images in terms of lateral distributions of elements. Magnetic sector mass analyzers, single-focusing as well as double focusing, play an important role while quadrupole and time-to-flight

instrumentation only account for a small fraction of instruments. Accelerator mass spectrometers, presumably the most exotic instruments, are a class of their own.

Ionization
Mostly, ionization conditions are harsh and simultaneously break up all molecular entities. Thus, atomic ions are delivered for elemental analysis. While some techniques only suffer from isobaric interferences of isotopes belonging to different elements, others may also be complicated by some molecular interferences. Especially plasma-based methods like GD-MS and ICP-MS are prone to formation of diatomic ions, mostly of the plasma gas, that may superimpose on atomic ions of the analyte.

Applications
In the past, the methodology has focused on metals, semiconductors, minerals, and gases. Element MS thus plays a major role in geological research, materials science, metallurgy, fabrication of electronic devices, oceanology, and climate studies, for example. Trace elemental analysis can reveal the geographical origin of a sample and isotope ratios may do the same. Also, isotope ratios can be used for determining the age of a sample, either of artwork or a prehistoric relic such as wood or bones of a dinosaur buried under sediment.

In the twenty-first century, samples of biological origin have gained relevance, especially as the combination of element MS and biomedical MS allows for the speciation, i.e., the assignment of elements to a specific molecule, typically a metal or semimetal to a certain protein.

Conclusion and Outlook
Mass spectrometry is no longer just organic, inorganic, physicochemical, biomedical, or environmental. On the contrary, mass spectrometry comprises a large number of facets and applications. The success of LA-ICP-MS, TOF-SIMS with polyatomic primary ion beams, and AMS in both the biomedical and the geological field marvelously exemplifies how a certain methodology can bridge the gap between extremes. The exploration of increasingly complex systems from cells and tissues to soils, ocean waters, and the atmosphere demands for the joint use of all techniques that enable crossing of interdisciplinary boundaries.

While working as a mass spectrometrist is necessarily correlated to a certain field of personal expertise, one should also be aware – at least to the degree of a good educational background in mass spectrometry – of the entire spectrum of this impressively versatile method – mass spectrometry, a domain of science in itself.

References

1. de Laeter JR, Kurz MD (2006) Alfred Nier and the Sector Field Mass Spectrometer. J Mass Spectrom 41:847–854. doi:10.1002/jms.1057

2. Budzikiewicz H, Grigsby RD (2006) Mass Spectrometry and Isotopes: A Century of Research and Discussion. Mass Spectrom Rev 25:146–157. doi:10.1002/mas.20061
3. Platzner IT, Habfast K, Walder AJ, Goetz APlatzner IT (eds) (1997) Modern Isotope Ratio Mass Spectrometry. Wiley, Chichester
4. Tuniz C, Bird JR, Fink D, Herzog GF (1998) Accelerator Mass Spectrometry – Ultrasensitive Analysis for Global Science. CRC Press, Boca Raton
5. Taylor HE (2000) Inductively Coupled Plasma Mass Spectroscopy. Academic Press, London
6. de Laeter JR (2001) Applications of Inorganic Mass Spectrometry. John Wiley & Sons, New York
7. Becker JS (2008) Inorganic Mass Spectrometry: Principles and Applications. John Wiley & Sons, Chichester
8. Prohaska T, Irrgeher J, Zitek A, Jakubowski N (eds) (2015) Sector Field Mass Spectrometry for Elemental and Isotopic Analysis. Royal Society of Chemistry, Cambridge
9. Douthitt CB (2008) Commercial Development of HR-ICPMS, MC-ICPMS and HR-GDMS. J Anal At Spectrom 23:685–689. doi:10.1039/B800341F
10. Hieftje GM (2008) Emergence and Impact of Alternative Sources and Mass Analyzers in Plasma Source Mass Spectrometry. J Anal At Spectrom 23:661–672. doi:10.1039/B717319A
11. de Laeter JR, De Bièvre P, Peiser HS (1992) Isotope Mass Spectrometry in Metrology. Mass Spectrom Rev 11:193–245. doi:10.1002/mas.1280110303
12. Ma R, Staton I, McLeod CW, Gomez MB, Gomez MM, Palacios MA (2001) Assessment of Airborne Platinum Contamination via ICP-Mass Spectrometric Analysis of Tree Bark. J Anal At Spectrom 16:1070–1075. doi:10.1039/B102940C
13. Stuewer D, Jakubowski N (1998) Elemental Analysis by Inductively Coupled Plasma Mass Spectrometry with Sector Field Instruments: A Progress Report. J Mass Spectrom 33:579–590. doi:10.1002/(SICI)1096-9888(199807)33:7<579::AID-JMS688>3.0.CO;2-W
14. Barker J, Garner RC (1999) Biomedical Applications of Accelerator Mass Spectrometry-Isotope Measurements at the Level of the Atom. Rapid Commun Mass Spectrom 13:285–293. doi:10.1002/(SICI)1097-0231(19990228)13:4<285::AID-RCM469>3.0.CO;2-R
15. Kutschera W (2005) Progress in Isotope Analysis at Ultra-Trace Level by AMS. Int J Mass Spectrom 242:145–160. doi:10.1016/j.ijms.2004.10.029
16. Becker JS, Zoriy M, Becker JS, Pickhardt C, Przybylski M (2004) Determination of Phosphorus and Metals in Human Brain Proteins After Isolation by Gel Electrophoresis by Laser Ablation Inductively Coupled Plasma Source Mass Spectrometry. J Anal At Spectrom 19:149–152. doi:10.1039/B311274H
17. Guenther D, Hattendorf B (2005) Solid Sample Analysis Using Laser Ablation Inductively Coupled Plasma Mass Spectrometry. Trends Anal Chem 24:255–265. doi:10.1016/j.trac.2004.11.017
18. Becker JS, Zoriy M, Becker JS, Dobrowolska J, Matusch A (2007) Laser Ablation Inductively Coupled Plasma Mass Spectrometry (LA-ICP-MS) in Elemental Imaging of Biological Tissues and in Proteomics. J Anal At Spectrom 22:736–744. doi:10.1039/B701558E
19. Cheah ELC, Koh HL (2008) Biomedical Applications of Accelerator Mass Spectrometry. Curr Anal Chem 4:102–110. doi:10.2174/157341108784587786
20. Becker JS, Matusch A, Wu B (2014) ioimaging Mass Spectrometry of Trace Elements – Recent Advance and Applications of LA-ICP-MS: A Review. Anal Chim Acta 835:1–18. doi:10.1016/j.aca.2014.04.048
21. Houk RS, Fassel VA, Flesch GD, Svec HJ, Gray AL, Taylor CE (1980) Inductively Coupled Argon Plasma as an Ion Source for Mass Spectrometric Determination of Trace Elements. Anal Chem 52:2283–2289. doi:10.1021/ac50064a012
22. Szpunar J (2004) Metallomics: A New Frontier in Analytical Chemistry. Anal Bioanal Chem 378:54–56. doi:10.1007/s00216-003-2333-z
23. Lobinski R, Schaumlöffel D, Szpunar J (2006) Mass Spectrometry in Bioinorganic Analytical Chemistry. Mass Spectrom Rev 25:255–289. doi:10.1002/mas.20069

24. Swart C, Jakubowski N (2016) Update on the Status of Metrology for Metalloproteins. J Anal At Spectrom 31:1756–1765. doi:10.1039/c6ja00181e
25. Walker AV (2008) Why Is SIMS Underused in Chemical and Biological Analysis? Challenges and Opportunities. Anal Chem 80:8865–8870. doi:10.1021/ac8013687
26. Cassiday L (2008) SIMS and MALDI: Better Together. Anal Chem 80:8860. doi:10.1021/ac8021828
27. Griffiths J (2008) Secondary Ion Mass Spectrometry. Anal Chem 80:7194–7197. doi:10.1021/ac801528u
28. McDonnell LA, Heeren RMA (2007) Imaging Mass Spectrometry. Mass Spectrom Rev 26:606–643. doi:10.1002/mas.20124
29. Adams F, Vertes A (1990) Inorganic Mass Spectrometry of Solid Samples. Fresenius J Anal Chem 337:638–647. doi:10.1007/BF00323098
30. Tanner SD, Baranov VI, Bandura DR (2002) Reaction Cells and Collision Cells for ICP-MS: a Tutorial Review. Spectrochim Acta, Part B 57B:1361–1452. doi:10.1016/S0584-8547(02)00069-1
31. Koppenaal DW, Eiden GC, Barinaga CJ (2004) Collision and Reaction Cells in Atomic Mass Spectrometry: Development, Status, and Applications. J Anal At Spectrom 19:561–570. doi:10.1039/B403510K
32. Becker JS, Dietze HJ (2000) Inorganic Mass Spectrometric Methods for Trace, Ultratrace, Isotope, and Surface Analysis. Int J Mass Spectrom 197:1–35. doi:10.1016/S1387-3806(99)00246-8
33. Richter S, Goldberg SA (2003) Improved Techniques for High Accuracy Isotope Ratio Measurements of Nuclear Materials Using Thermal Ionization Mass Spectrometry. Int J Mass Spectrom 229:181–197. doi:10.1016/S1387-3806(03)00338-5
34. Encinar JR, Ouerdane L, Buchmann W, Tortajada J, Lobinski R, Szpunar J (2003) Identification of Water-Soluble Selenium-Containing Proteins in Selenized Yeast by Size-Exclusion-Reversed-Phase HPLC-ICP-MS Followed by MALDI-TOF and Electrospray Q-TOF Mass Spectrometry. Anal Chem 75:3765–3774. doi:10.1021/ac034103m
35. Halas S, Durakiewicz T (1998) Filament Temperature Stabilizer for a Thermal Ionization Mass Spectrometer. Int J Mass Spectrom 181:167–171. doi:10.1016/S1387-3806(98)14186-6
36. Kawano H, Page FM (1983) Experimental Methods and Techniques for Negative-Ion Production by Surface Ionization. Part I. Fundamental Aspects of Surface Ionization. Int J Mass Spectrom Ion Phys 50:1–33. doi:10.1016/0020-7381(83)80001-1
37. Kawano H, Hidaka Y, Page FM (1983) Experimental Methods and Techniques for Negative-Ion Production by Surface Ionization. Part II. Instrumentation and Operation. Int J Mass Spectrom Ion Phys 50:35–75. doi:10.1016/0020-7381(83)80002-3
38. Heumann KG, Schindlmeier W, Zeininger H, Schmidt M (1985) Application of an Economical and Small Thermal Ionization Mass Spectrometer for Accurate Anion Trace Analyses. Fresenius Z Anal Chem 320:457–462. doi:10.1007/BF00479812
39. Heumann KG, Kastenmayer P, Zeininger H (1981) Lead and Thallium Trace Determination in the ppm and ppb Range in Biological Material by Mass Spectrometric Isotope Dilution Analysis. Fresenius Z Anal Chem 306:173–177. doi:10.1007/BF00482091
40. Waidmann E, Emons H, Duerbeck HW (1994) Trace Determination of Tl, Cu, Pb, Cd, and Zn in Specimens of the Limnic Environment Using Isotope Dilution Mass Spectrometry with Thermal Ionization. Fresenius J Anal Chem 350:293–297. doi:10.1007/BF00322485
41. Schade U, Stoll R, Röllgen FW (1983) Thermal Surface Ionization Mass Spectrometry of Organic Salts. Int J Mass Spectrom Ion Phys 46:337–340. doi:10.1016/0020-7381(83)80121-1
42. Moens L (1997) Applications of Mass Spectrometry in the Trace Element Analysis of Biological Materials. Fresenius J Anal Chem 359:309–316. doi:10.1007/s002160050579
43. Koppenaal DW (1990) Atomic Mass Spectrometry. Anal Chem 62:303R–324R. doi:10.1021/ac00211a015

44. Verlinden J, Gijbels R, Adams F (1986) Application of Spark-Source Mass Spectrometry in the Analysis of Semiconductor Materials. A Review. J Anal At Spectrom 1:411–419. doi:10.1039/JA9860100411
45. Jochum KP (1997) Elemental analysis by spark source mass spectrometry. In: Gill R (ed) Modern Analytical Geochemistry. Addison Wesley/Longman, Harlow
46. Jochum KP, Stoll B, Pfänder JA, Seufert M, Flanz M, Maissenbacher P, Hofmann M, Hofmann AW (2001) Progress in Multi-Ion Counting Spark-Source Mass Spectrometry (MIC-SSMS) for the Analysis of Geological Samples. Fresenius J Anal Chem 370:647–653. doi:10.1007/s002160100786
47. Saprykin AI, Becker JS, Dietze HJ (1999) Investigation of the Analytical Performance of Gliding Spark Source Mass Spectrometry (GSSMS) for the Trace Analysis of Nonconducting Materials. Fresenius J Anal Chem 364:763–767. doi:10.1007/s002160051429
48. Hoffmann V, Kasik M, Robinson PK, Venzago C (2005) Glow Discharge Mass Spectrometry. Anal Bioanal Chem 381:173–188. doi:10.1007/s00216-004-2933-2
49. Wiedemann B, Alt HC, Meyer JD, Michelmann RW, Bethge K (1999) Spark Source Mass Spectrometric Calibration of the Local Vibrational Mode Absorption of Carbon in Gallium Arsenide on Arsenic Sublattice Sites. Fresenius J Anal Chem 364:768–771. doi:10.1007/s002160051430
50. Gijbels R, Bogaerts A (1997) Recent Trends in Solid Mass Spectrometry. GDMS and Other Methods. Fresenius J Anal Chem 359:326–330. doi:10.1007/s002160050581
51. Stuewer D (1990) Glow Discharge Mass Spectrometry – A Versatile Tool for Elemental Analysis. Fresenius J Anal Chem 337:737–742. doi:10.1007/BF00322247
52. Marcus RK, King FL Jr, Harrison WW (1986) Hollow Cathode Plume as an Atomization/Ionization Source for Solids Mass Spectrometry. Anal Chem 58:972–974. doi:10.1021/ac00295a067
53. Harrison WW, Hess KR, Marcus RK, King FL (1986) Glow Discharge Mass Spectrometry. Anal Chem 58: 341A–342A, 344A, 346A, 348A, 350A, 352A. doi: 10.1021/ac00293a002
54. Duckworth DC, Marcus RK (1989) Radio Frequency Powered Glow Discharge Atomization/Ionization Source for Solids Mass Spectrometry. Anal Chem 61:1879–1886. doi:10.1021/ac00192a020
55. Marcus RK (1994) Radiofrequency Powered Glow Discharges for Emission and Mass Spectrometry: Operating Characteristics, Figures of Merit and Future Prospects. J Anal At Spectrom 9:1029–1037. doi:10.1039/JA9940901029
56. Marcus RK (1996) Radiofrequency Powered Glow Discharges: Opportunities and Challenges. Plenary Lecture. J Anal At Spectrom 11:821–828. doi:10.1039/JA9961100821
57. Jakubowski N, Prohaska T, Rottmann L, Vanhaecke F (2011) Inductively Coupled Plasma- and Glow Discharge Plasma-Sector Field Mass Spectrometry, Part I. Tutorial: Fundamentals and Instrumentation. J Anal At Spectrom 26:693–726. doi:10.1039/c0ja00161a
58. Jakubowski N, Prohaska T, Vanhaecke F, Roos PH, Lindemann T (2011) Inductively Coupled Plasma- and Glow Discharge Plasma-Sector Field Mass Spectrometry, Part II. Applications. J Anal At Spectrom 26:727–757. doi:10.1039/c0ja00007h
59. Harrison WW, Klingler JA, Ratliff PH, Mei Y, Barshick CM (1990) Glow Discharge Techniques in Analytical Chemistry. Anal Chem 62:943A–949A. doi:10.1021/ac00217a001
60. King FL, Harrison WW (1990) Glow Discharge Mass Spectrometry: an Introduction to the Technique and Its Utility. Mass Spectrom Rev 9:285–317. doi:10.1002/mas.1280090303
61. Bogaerts A, Gijbels R (1999) New Developments and Applications in GDMS. Fresenius J Anal Chem 364:367–375. doi:10.1007/s002160051352
62. Nelis T, Pallosi J (2006) Glow Discharge as a Tool for Surface and Interface Analysis. Appl Spectrosc Rev 41:227–258. doi:10.1080/05704920600620345
63. Jakubowski N, Dorka R, Steers E, Tempez A (2007) Trends in Glow Discharge Spectroscopy. J Anal At Spectrom 22:722–735. doi:10.1039/B705238N
64. Penning FM (1927) Über Ionisation durch metastabile Atome. Naturwissenschaften 15:818. doi:10.1007/BF01505431

65. Bogaerts A (1999) The Glow Discharge: an Exciting Plasma! J Anal At Spectrom 14:1375–1384. doi:10.1039/A900772E
66. Xing Y, Xiaojia L, Haizhou W (2008) Determination of Trace Elements and Correction of Mass Spectral Interferences in Superalloy Analyzed by Glow Discharge Mass Spectrometry. Eur J Mass Spectrom 14:211–218. doi:10.1255/ejms.930
67. Winchester MR, Payling R (2004) Radio-Frequency Glow Discharge Spectrometry: A Critical Review. Spectrochim Acta, Part B 59B:607–666. doi:10.1016/j.sab.2004.02.013
68. Majidi V, Moser M, Lewis C, Hang W, King FL (2000) Explicit Chemical Speciation by Microsecond Pulsed Glow Discharge Time-of-Flight Mass Spectrometry: Concurrent Acquisition of Structural, Molecular and Elemental Information. J Anal At Spectrom 15:19–25. doi:10.1039/A905477D
69. Lewis CL, Moser MA, Dale DE Jr, Hang W, Hassell C, King FL, Majidi V (2003) Time-Gated Pulsed Glow Discharge: Real-Time Chemical Speciation at the Elemental, Structural, and Molecular Level for Gas Chromatography Time-of-Flight Mass Spectrometry. Anal Chem 75:1983–1996. doi:10.1021/ac026242u
70. Fliegel D, Fuhrer K, Gonin M, Guenther D (2006) Evaluation of a Pulsed Glow Discharge Time-of-Flight Mass Spectrometer as a Detector for Gas Chromatography and the Influence of the Glow Discharge Source Parameters on the Information Volume in Chemical Speciation Analysis. Anal Bioanal Chem 386:169–179. doi:10.1007/s00216-006-0515-1
71. Nagulin KY, Akhmetshin DS, Gilmutdinov AK, Ibragimov RA (2015) Three-Dimensional Modeling and Schlieren Visualization of Pure Ar Plasma Flow in Inductively Coupled Plasma Torches. J Anal At Spectrom 30:360–367. doi:10.1039/c4ja00254g
72. Bandura DR, Baranov VI, Tanner SD (2001) Reaction Chemistry and Collisional Processes in Multipole Devices for Resolving Isobaric Interferences in ICP-MS. Fresenius J Anal Chem 370:454–470. doi:10.1007/s002160100869
73. Wilbur S (2008) A Pragmatic Approach to Managing Interferences in ICP-MS. Spectroscopy 23:18–23
74. Aeschliman DB, Bajic SJ, Baldwin DP, Houk RS (2003) High-Speed Digital Photographic Study of an Inductively Coupled Plasma During Laser Ablation: Comparison of Dried Solution Aerosols from a Microconcentric Nebulizer and Solid Particles from Laser Ablation. J Anal At Spectrom 18:1008–1014. doi:10.1039/b302546m
75. Becker JS, Dietze HJ (1999) Application of Double-Focusing Sector Field ICP Mass Spectrometry with Shielded Torch Using Different Nebulizers for Ultratrace and Precise Isotope Analysis of Long-Lived Radionuclides. J Anal At Spectrom 14:1493–1500. doi:10.1039/A901762C
76. Myers DP, Hieftje GM (1993) Preliminary Design Considerations and Characteristics of an Inductively Coupled Plasma-Time-of-Flight Mass Spectrometer. Microchem J 48:259–277. doi:10.1006/mchj.1993.1102
77. Myers DP, Li G, Yang P, Hieftje GM (1994) An Inductively Coupled Plasma-Time-of-Flight Mass Spectrometer for Elemental Analysis. Part I: Optimization and Characteristics. J Am Soc Mass Spectrom 5:1008–1016. doi:10.1016/1044-0305(94)80019-7
78. Myers DP, Mahoney PP, Li G, Hieftje GM (1995) Isotope Ratios and Abundance Sensitivity Obtained with an Inductively Coupled Plasma-Time-of-Flight Mass Spectrometer. J Am Soc Mass Spectrom 6:920–927. doi:10.1016/1044-0305(95)00484-U
79. Hieftje GM, Myers DP, Li G, Mahoney PP, Burgoyne TW, Ray SJ, Guzowski JP (1997) Toward the Next Generation of Atomic Mass Spectrometers. J Anal At Spectrom 12:287–292. doi:10.1039/A605067K
80. Westphal CS, McLean JA, Acon BW, Allen LA, Montaser A (2002) Axial Inductively Coupled Plasma Time-of-Flight Mass Spectrometry Using Direct Liquid Sample Introduction. J Anal At Spectrom 17:669–675. doi:10.1039/B200771C
81. Tanner M, Guenther D (2008) Measurement and Readout of Mass Spectra with 30 μs Time Resolution, Applied to In-Torch LA-ICP-MS. Anal Bioanal Chem 391:1211–1220. doi:10.1007/s00216-008-1869-3

82. Milgram KE, White FM, Goodner KL, Watson CH, Koppenaal DW, Barinaga CJ, Smith BH, Winefordner JD, Marshall AG, Houk RS, Eyler JR (1997) High-Resolution Inductively Coupled Plasma Fourier Transform Ion Cyclotron Resonance Mass Spectrometry. Anal Chem 69:3714–3721. doi:10.1021/ac970126n
83. Becker JS, Dietze HJ (1998) Ultratrace and Precise Isotope Analysis by Double-Focusing Sector Field Inductively Coupled Plasma Mass Spectrometry. J Anal At Spectrom 13:1057–1063. doi:10.1039/A801528G
84. Yang L (2009) Accurate and Precise Determination of Isotopic Ratios by MC-ICP-MS: A Review. Mass Spectrom Rev 28:990–1011. doi:10.1002/mas.20251
85. Ardelt D, Polatajko A, Primm O, Reijnen M (2013) Isotope Ratio Measurements with a Fully Simultaneous Mattauch-Herzog ICP-MS. Anal Bioanal Chem 405:2987–2994. doi:10.1007/s00216-012-6543-0
86. Mahoney PP, Li G, Hieftje GM (1996) Laser Ablation-Inductively Coupled Plasma Mass Spectrometry with a Time-of-Flight Mass Analyzer. J Anal At Spectrom 11:401–405. doi:10.1039/JA9961100401
87. Pisonero J, Kroslakova I, Guenther D, Latkoczy C (2006) Laser Ablation Inductively Coupled Plasma Mass Spectrometry for Direct Analysis of the Spatial Distribution of Trace Elements in Metallurgical-Grade Silicon. Anal Bioanal Chem 386:12–20. doi:10.1007/s00216-006-0658-0
88. Neilsen JL, Abildtrup A, Christensen J, Watson P, Cox A, McLeod CW (1998) Laser Ablation Inductively Coupled Plasma-Mass Spectrometry in Combination with Gel Electrophoresis: A New Strategy for Speciation of Metal Binding Serum Proteins. Spectrochim Acta, Part B 53B:339–345. doi:10.1016/S0584-8547(98)00077-9
89. Chery CC, Moens L, Cornelis R, Vanhaecke F (2006) Capabilities and Limitations of Gel Electrophoresis for Elemental Speciation: A Laboratory's Experience. Pure Appl Chem 78:91–103. doi:10.1351/pac200678010091
90. Konz I, Fernandez B, Fernandez ML, Pereiro R, Gonzalez-Iglesias H, Coca-Prados M, Sanz-Medel A (2014) Quantitative Bioimaging of Trace Elements in the Human Lens by LA-ICP-MS. Anal Bioanal Chem 406:2343–2348. doi:10.1007/s00216-014-7617-y
91. Benninghoven A (1975) Developments in Secondary Ion Mass Spectroscopy and Applications to Surface Studies. Surf Sci 53:596–625. doi:10.1016/0039-6028(75)90158-2
92. Pachuta SJ, Cooks RG (1987) Mechanisms in Molecular SIMS. Chem Rev 87:647–669. doi:10.1021/cr00079a009
93. Benninghoven A, Werner HW, Rudenauer FG (eds) (1987) Secondary Ion Mass Spectrometry: Basic Concepts, Instrumental Aspects, Applications and Trends. Wiley Interscience, New York
94. Briggs D, Brown A, Vickerman JC (1989) Handbook of Static Secondary Ion Mass Spectrometry. Wiley, Chichester
95. Arnot FL, Beckett C (1938) Formation of Negative Ions at Surfaces. Nature 141:1011–1012. doi:10.1038/1411011c0
96. Arnot FL, Milligan JC (1936) A New Process of Negative-Ion Formation. Proc R Soc A 156:538–560. doi:10.1098/rspa.1936.0166
97. Herzog RFK, Viehbock FP (1949) Ion Source for Mass-Spectrography. Phys Rev 76:855–856. doi:10.1103/PhysRev.76.855
98. Benninghoven A (1969) Mechanism of Ion Formation and Ion Emission During Sputtering. Z Phys 220:159–180. doi:10.1007/BF01394745
99. Benninghoven A (1970) Analysis of Monomolecular Surface Layers of Solids by Secondary Ion Emission. Z Phys 230:403–417. doi:10.1007/BF01394486
100. Adams F (2008) Analytical Atomic Spectrometry and Imaging: Looking Backward from 2020 to 1975. Spectrochim Acta, Part B 63B:738–745. doi:10.1016/j.sab.2008.05.001
101. Benninghoven A, Sichtermann WK (1978) Detection, Identification and Structural Investigation of Biologically Important Compounds by Secondary Ion Mass Spectrometry. Anal Chem 50:1180–1184. doi:10.1021/ac50030a043

102. Coath CD, Long JVP (1995) A High-Brightness Duoplasmatron Ion Source for Microprobe Secondary-Ion Mass Spectrometry. Rev Sci Instrum 66:1018–1023. doi:10.1063/1.1146038
103. Konarski P, Kalczuk M, Koscinski J (1992) Bakeable Duoplasmatron Ion Gun for SIMS Microanalysis. Rev Sci Instrum 63:2397–2399. doi:10.1063/1.1142941
104. Pacholski ML, Winograd N (1999) Imaging with Mass Spectrometry. Chem Rev 99:2977–3005. doi:10.1021/cr980137w
105. Weibel D, Wong S, Lockyer N, Blenkinsopp P, Hill R, Vickerman JC (2003) A C_{60} Primary Ion Beam System for Time of Flight Secondary Ion Mass Spectrometry: Its Development and Secondary Ion Yield Characteristics. Anal Chem 75:1754–1764. doi:10.1021/ac026338o
106. Chait BT, Standing KG (1981) A Time-of-Flight Mass Spectrometer for Measurement of Secondary Ion Mass Spectra. Int J Mass Spectrom Ion Phys 40:185–193. doi:10.1016/0020-7381(81)80041-1
107. Standing KG, Chait BT, Ens W, McIntosh G, Beavis R (1982) Time-of-Flight Measurements of Secondary Organic Ions Produced by 1 keV to 16 keV Primary Ions. Nucl Instrum Methods Phys Res 198:33–38. doi:10.1016/0167-5087(82)90048-5
108. Jabs HU, Assmann G, Greifendorf D, Benninghoven A (1986) High Performance Liquid Chromatography and Time-of-Flight Secondary Ion Mass Spectrometry: A New Dimension in Structural Analysis of Apolipoproteins. J Lipid Res 27:613–621
109. Ens W, Standing KG, Chait BT, Field FH (1981) Comparison of Mass Spectra Obtained with Low-Energy Ion and High-Energy ^{252}Californium Fission Fragment Bombardment. Anal Chem 53:1241–1244. doi:10.1021/ac00231a026
110. Lafortune F, Beavis R, Tang X, Standing KG, Chait BT (1987) Narrowing the Gap Between KeV and Fission Fragment Secondary Ion Yields with Nitrocellulose. Rapid Commun Mass Spectrom 1:114–116. doi:10.1002/rcm.1290010707
111. Ens W, Main DE, Standing KG, Chait BT (1988) Comparison of Relative Quasi-Molecular Ion Yields for 8-keV Ion and ^{252}Cf Fission Fragment Bombardment. Anal Chem 60:1494–1498. doi:10.1021/ac00166a004
112. Olthoff JK, Honovich JP, Cotter RJ (1987) Liquid Secondary Ion Time-of-Flight Mass Spectrometry. Anal Chem 59:999–1002. doi:10.1021/ac00134a016
113. Linton RW, Mawn MP, Belu AM, DeSimone JM, Hunt MO Jr, Menceloglu YZ, Cramer HG, Benninghoven A (1993) Time-of-Flight Secondary Ion Mass Spectrometric Analysis of Polymer Surfaces and Additives. Surf Interface Anal 20:991–999. doi:10.1002/sia.740201210
114. Galuska AA (1997) ToF-SIMS Determination of Molecular Weights from Polymeric Surfaces and Microscopic Phases. Surf Interface Anal 25:790–798. doi:10.1002/(SICI)1096-9918(199709)25:10<790::AID-SIA301>3.0.CO;2-F
115. Bullett NA, Short RD, O'Leary T, Beck AJ, Douglas CWI, Cambray-Deakin M, Fletcher IW, Roberts A, Blomfield C (2001) Direct Imaging of Plasma-Polymerized Chemical Micropatterns. Surf Interface Anal 31:1074–1076. doi:10.1002/sia.1146
116. Liu S, Weng LT, Chan CM, Li L, Ho NK, Jiang M (2001) Quantitative Surface Characterization of Poly(styrene)/Poly(4-vinyl phenol) Random and Block Copolymers by ToF-SIMS and XPS. Surf Interface Anal 31:745–753. doi:10.1002/sia.1105
117. Médard N, Poleunis C, Vanden Eynde X, Bertrand P (2002) Characterization of Additives at Polymer Surfaces by TOF-SIMS. Surf Interface Anal 34:565–569. doi:10.1002/sia.1361
118. Davies N, Weibel DE, Blenkinsopp P, Lockyer N, Hill R, Vickerman JC (2003) Development and Experimental Application of a Gold Liquid Metal Ion Source. Appl Surf Sci 203-204:223–227. doi:10.1016/S0169-4332(02)00631-1
119. Nagy G, Walker AV (2007) Enhanced Secondary Ion Emission with a Bismuth Cluster Ion Source. Int J Mass Spectrom 262:144–153. doi:10.1016/j.ijms.2006.11.003
120. Touboul D, Kollmer F, Niehuis E, Brunelle A, Laprevote O (2005) Improvement of Biological Time-of-Flight-Secondary Ion Mass Spectrometry Imaging with a Bismuth Cluster Ion Source. J Am Soc Mass Spectrom 16:1608–1618. doi:10.1016/j.jasms.2005.06.005

121. Malmberg P, Nygren H (2008) Methods for the Analysis of the Composition of Bone Tissue, with a Focus on Imaging Mass Spectrometry (TOF-SIMS). Proteomics 8:3755–3762. doi:10.1002/pmic.200800198
122. Wong SCC, Hill R, Blenkinsopp P, Lockyer NP, Weibel DE, Vickerman JC (2003) Development of a C_{60}^+ Ion Gun for Static SIMS and Chemical Imaging. Appl Surf Sci 203-204:219–222. doi:10.1016/S0169-4332(02)00629-3
123. Fletcher JS, Lockyer NP, Vickerman JC (2006) C_{60}, Buckminsterfullerene: Its Impact on Biological ToF-SIMS Analysis. Surf Interface Anal 38:1393–1400. doi:10.1002/sia.2461
124. Mas S, Perez R, Martinez-Pinna R, Egido J, Vivanco F (2008) Cluster TOF-SIMS Imaging: A New Light for in Situ Metabolomics? Proteomics 8:3735–3745. doi:10.1002/pmic.200800115
125. Briggs D, Hearn MJ (1985) Analysis of Polymer Surfaces by SIMS. Part 5. The Effects of Primary Ion Mass and Energy on Secondary Ion Relative Intensities. Int J Mass Spectrom Ion Proc 67:47–56. doi:10.1016/0168-1176(85)83036-6
126. Brunelle A, Laprevote O (2009) Lipid Imaging with Cluster Time-of-Flight Secondary Ion Mass Spectrometry. Anal Bioanal Chem 393:31–35. doi:10.1007/s00216-008-2367-3
127. Herrmann AM, Ritz K, Nunan N, Clode PL, Pett-Ridge J, Kilburn MR, Murphy DV, O'Donnell AG, Stockdale EA (2007) Nano-Scale Secondary Ion Mass Spectrometry – A New Analytical Tool in Biogeochemistry and Soil Ecology: A Review Article. Soil Biol Biochem 39:1835–1850. doi:10.1016/j.soilbio.2007.03.011
128. Fletcher JS, Rabbani S, Henderson A, Blenkinsopp P, Thompson SP, Lockyer NP, Vickerman JC (2008) A New Dynamic in Mass Spectral Imaging of Single Biological Cells. Anal Chem 80:9058–9064. doi:10.1021/ac8015278
129. Carado A, Passarelli MK, Kozole J, Wingate JE, Winograd N, Loboda AV (2008) C_{60} Secondary Ion Mass Spectrometry with a Hybrid-Quadrupole Orthogonal Time-of-Flight Mass Spectrometer. Anal Chem 80:7921–7929. doi:10.1021/ac801712s
130. Hellborg R, Skog G (2008) Accelerator Mass Spectrometry. Mass Spectrom Rev 27:398–427. doi:10.1002/mas.20172
131. Suter M (2004) 25 Years of AMS – A Review of Recent Developments. Nucl Instr Methods Phys Res B 223-224:139–148. doi:10.1016/j.nimb.2004.04.030
132. Stocker M, Doebeli M, Grajcar M, Suter M, Synal HA, Wacker L (2005) A Universal and Competitive Compact AMS Facility. Nucl Instr Methods Phys Res B 240:483–489. doi:10.1016/j.nimb.2005.06.224
133. Wacker L, Fifield LK, Olivier S, Suter M, Synal HA (2006) Compact Accelerator Mass Spectrometry: A Powerful Tool to Measure Actinides in the Environment. Spec Publ R Soc Chem 305:44–46
134. Nelson DE, Korteling RG, Stott WR (1977) Carbon-14: Direct Detection at Natural Concentrations. Science 198:507–508. doi:10.1126/science.198.4316.507
135. Bennett CL, Beukens RP, Clover MR, Grove HE, Liebert RB, Litherland AE, Purser KH, Sondheim WE (1977) Radiocarbon Dating Using Electrostatic Accelerators: Negative Ions Provide the Key. Science 198:508–510. doi:10.1126/science.198.4316.508
136. Lappin G, Garner RC (2004) Current Perspectives of ^{14}C-Isotope Measurement in Biomedical Accelerator Mass Spectrometry. Anal Bioanal Chem 378:356–364. doi:10.1007/s00216-003-2348-5
137. Brown K, Dingley KH, Turteltaub KW (2005) Accelerator Mass Spectrometry for Biomedical Research. Methods Enzymol 402:423–443. doi:10.1016/S0076-6879(05)02014-8
138. Ikeda T (2005) Instruments for Radiation Measurement in Life Sciences. VI. Use of accelerator mass spectrometry in studies on drug metabolism and pharmacokinetics. Radioisotopes 54:15–21. doi:10.3769/radioisotopes.54.15
139. Brown K, Tompkins EM, White INH (2006) Applications of Accelerator Mass Spectrometry for Pharmacological and Toxicological Research. Mass Spectrom Rev 25:127–145. doi:10.1002/mas.20059